[redacted]

FILE # 0221

Final Report

DEMONSTRATION AUTOMATIC FOCUSING REAR-SCREEN PROJECTOR

STAT [redacted]

Declass Review by NIMA/DOD

STAT

[redacted]

February 1968

Final Report

DEMONSTRATION AUTOMATIC FOCUSING REAR-SCREEN PROJECTOR

STAT

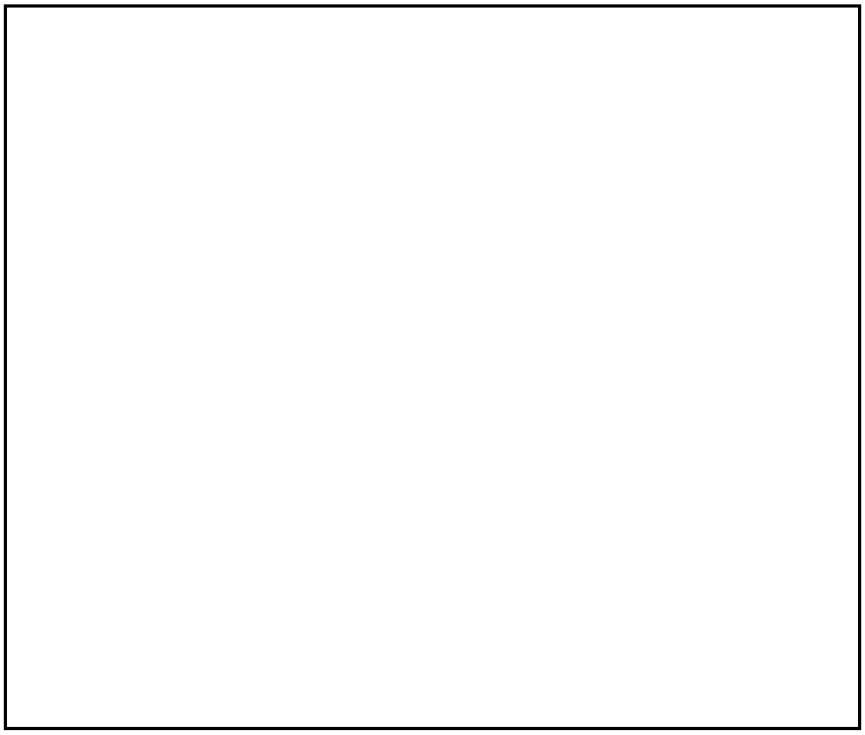

Copy No. 13

Approved For Release 2003/01/28 : CIA-RDP78B04770A002000040013-3

ABSTRACT

A functioning demonstration rear-screen projector with automatic focus detection and control was constructed and tested. Satisfactory performance was obtained at 3× magnification with a typical film scanning speed of 2 inches per second. Two methods for extending the automatic focus to higher magnifications are described and evaluated. The sources of error for the focus-detection subsystem are discussed and the techniques required to eliminate or reduce the errors are described. A comprehensive review of the focus-detection theory is presented in an Appendix.

CONTENTS

ILLUSTRATIONS

TABLES

I INTRODUCTION

A recent research project at [redacted] covered the detailed analytical and preliminary laboratory work for development of automatic focus detection techniques applicable to rear-screen projectors of the type used to scan aerial photographs.[1]* The conclusions of this investigation included the technical feasibility of building a working demonstration projector combining the basic elements of a rear-screen projector with a focus-detection subsystem and a lens focus servo subsystem, thereby permitting study of the problems and compromises necessary to achieve a successful system. The understanding thus gained could be used to guide the application of focus-detection theory and the development of the related subsystems needed to build a successful operational system.

STAT

Accordingly, the purpose of the present project has been to construct a working projector using, wherever possible, existing components and techniques. Research emphasis has been placed on problems of integration, rather than on the refinement and optimization of any one subsystem.

Section II of this report describes each of the major subsystems used in the projector. Specific problems resulting from integration of the focus detection and lens servo subsystems into a complete projector are discussed in Sec. III. The measured performance of the projector at 3× magnification is presented in Sec. IV, along with a detailed discussion of two different approaches for extending the application of focus-detection techniques to higher magnifications. Conclusions and recommendations are presented in Sec. V. The basic lens servo specifications and circuitry are given in Appendix A. Appendix B presents a refined presentation of the basic focus-detection theory.

---

*References are listed at the end of the report.

II DESCRIPTION OF THE DEMONSTRATION REAR-SCREEN PROJECTOR

The demonstration projector contains all the primary functioning subsystems required to permit the projection of the image from a 9 X 9 inch section of a roll of aerial film onto a 27 X 27 inch rear-projection screen. (An overall layout of the projector is shown in Fig. 10 at the end of this section.)

A. Film Transport Subsystem

The film transport is driven by an electronically controlled motor, which permits the drive speed to be varied over the practical range of scanning speeds from zero to greater than 4 inches per second. A simplified layout of the film drive is shown in Fig. 1; a photograph of the unit used in the demonstration model is shown in Fig. 2.

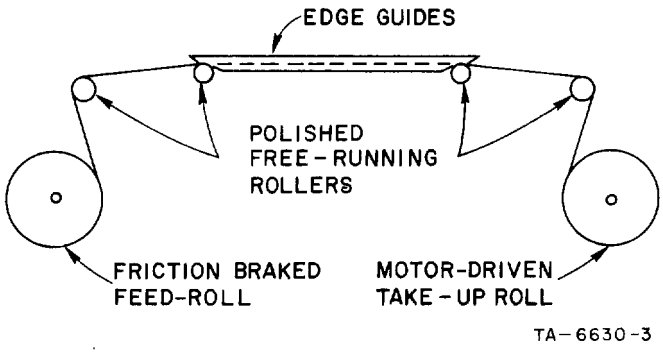

FIG. 1 SIMPLIFIED LAYOUT OF FILM DRIVE SUBSYSTEM

The film is guided by polished rollers and, in the critical projection area between the two center rollers, by spring-tensioned edge guides along the outer 1/8 inch of the film. Within the frame defined by the inner rollers and edge guides, the film tends to depart from the plane defined by the edges. A variety of factors influence the magnitude, frequency, and spatial distribution of the film variations. Key factors include such film base characteristics as thickness, tendency to curl, and mechanical distortions in the film; these imperfections

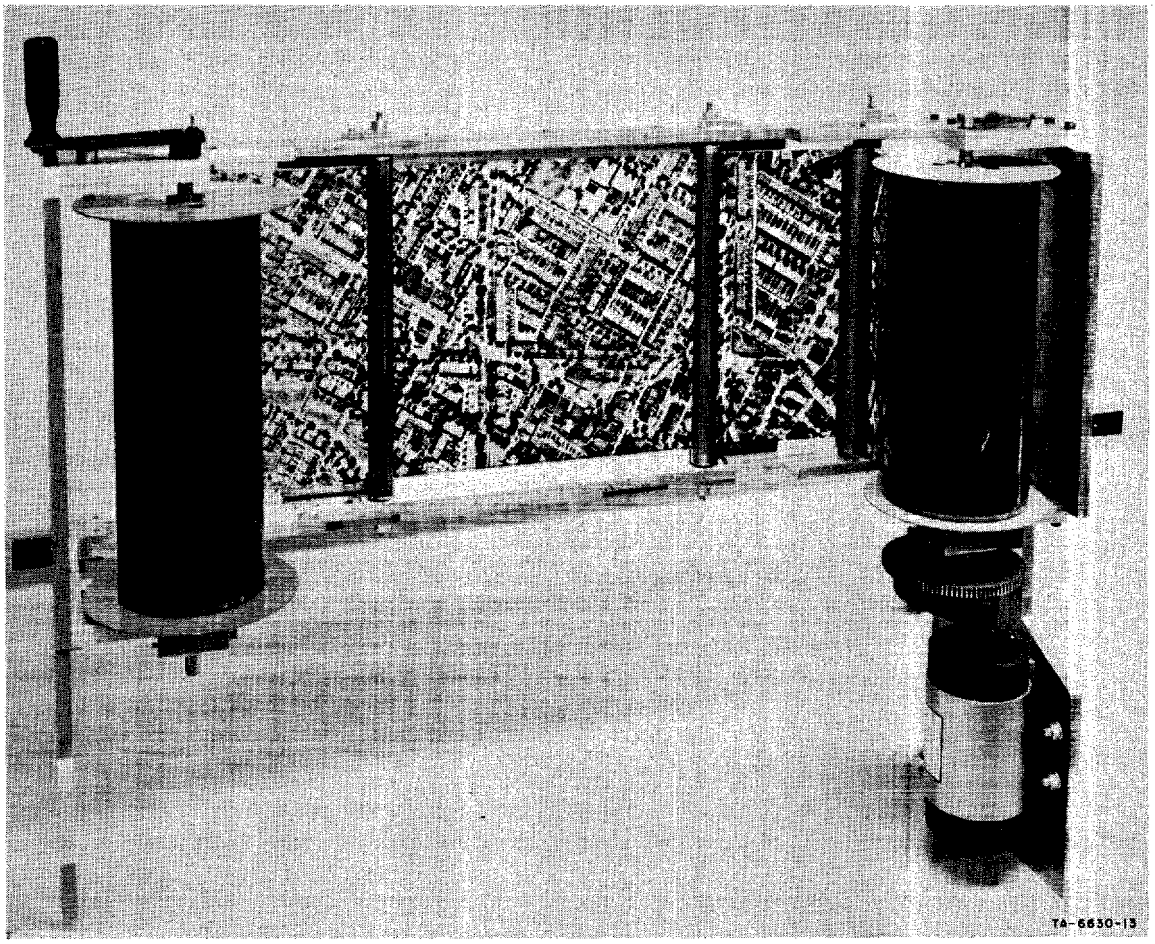

FIG. 2 FILM DRIVE SUBSYSTEM

result in uneven drive tensions in the film, which in turn produce wrinkling of the film plane. The relationship of these characteristics to the film drive tension, the guiding techniques employed, and the scanning speed used have a significant influence on the film variations occurring during scanning operations.

The selected design for the demonstration projector was based on the following criteria:

(1) The film guidance techniques should be applicable to future projectors; implicit in this criterion is the requirement that the film must in no manner be damaged by passing through the projector.

(2) The film drive should provide a useful range of film scanning speeds and resultant characteristics of film movement to provide a realistic test for the focus control subsystem.

(3) The film drive must be simple, i.e., inexpensive and easy to construct. Therefore, a number of features that would be required for operational use were not included. High-speed slewing, motor-driven reverse winding, and X-Y positioning of the entire film carriage were therefore neglected as not fundamental to testing the automatic focus operation.

(4) The film guidance system should not employ glass platens either to provide a thin air film constraint of the film during scanning or to clamp the film during stationary viewing. The use of such platens would restrict the evaluation of the focus-detection techniques to a limited range of film motions.

While the performance of the film drive at a steady film speed of 2 in/s is very good, the simple friction braking on the drive and feed rolls results in a different film tension during steady film motion from the tension when the film is stopped, and the tendency of the film base to produce buckling or curling results in different central film plane positions at different tensions. Additionally, the resonant frequency of the film is a function of the tension. As the tension--and hence the resonant frequency--is varied, the effect of external excitation frequencies varies. Further research should be undertaken to study the film and film drive characteristics and their relationship to the overall characteristics and requirements of rear-screen, automatic-focusing projectors.

B. Light Source

The projector light source is the lamphouse portion of a [redacted] STAT Model V-184 8 × 10 inch enlarger. The flexibility and availability

of this unit made it a suitable light source of the demonstration projector: The condensers within the lamphouse are suitable for illuminating a 9 × 9 inch film frame for projection. A satisfactory average screen illumination level of between 15 to 20 footlamberts was obtained at 3× magnification using the normal 300-W light source. Condensers of alternative focal length and higher powered light sources are available, permitting increased illumination of the screen for higher magnifications.

During the course of the project, a technique was suggested for achieving higher magnifications to allow detailed inspection of areas selected during the scanning (3×) mode. The technique requires that a small hole be cut in the viewing screen; the image formed in this area is examined with a small magnifier, thereby permitting high-resolution, high-power examination. Since the image is viewed directly through the magnifier, it is desirable to provide diffuse illumination of the film in this area. This was accomplished in the demonstration model by attaching a 5/8-inch square piece of ground glass to the center of the condenser lens located just behind the film plane. This diffusely illuminated area of the film frame corresponds to a hole approximately 2 inches square cut in the projection screen. The details of the attachment and the shape of the ground glass used for the illumination of the center area of the film are described in detail in Sec. III-A-2-a.

C. Lens and Lens Servo System

Figure 3 shows a photograph of the lens servo assembly. The details of the electronics and the design specifications for the servo and its performance are given in Appendix A.* The projection lens used is a [redacted] enlarging lens, f/5.6, with a focal length of 12 inches. This provides a 3× magnification with adequate resolution for both the operation of the focus-detection system and for visual evaluation of the overall system performance.

STAT

*The lens servo was designed and tested by [redacted] STAT

[redacted] STAT

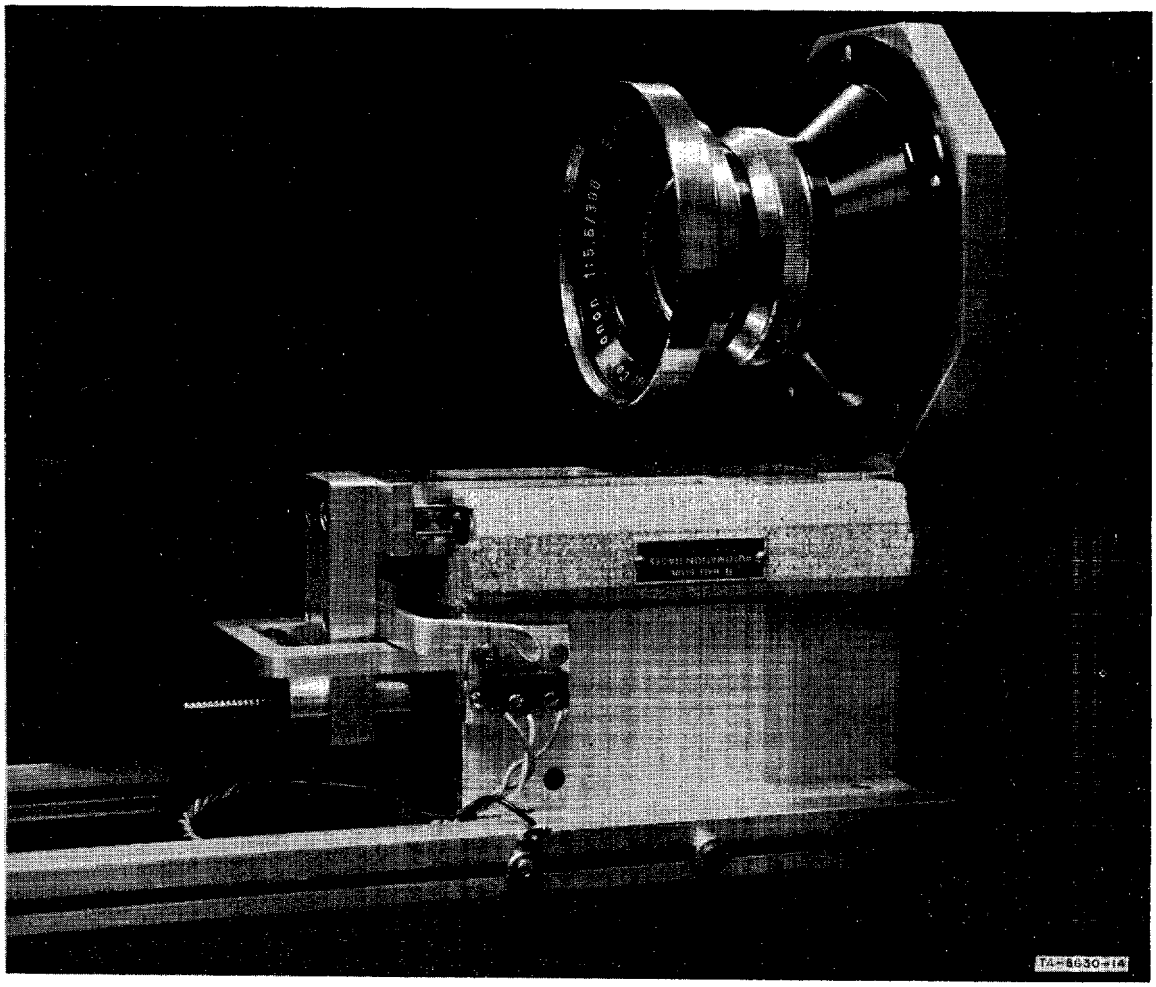

FIG. 3 LENS SERVO ASSEMBLY

The lens is mounted on an Automation Gages Ball-Slide linear motion guideway driven by a 16-turn/inch lead screw. Two back-to-back spring-loaded ball bearing nuts minimize backlash. The lead screw is directly driven by a Kerfott R 801-1A servo motor/tachometer combination.

D. Focus-Detection Subsystem

1. Description

The focus-detection subsystem (Fig. 4) consists of the following components:

The focus-detection masks used for this unit are single, straight edges of 0.001-inch thick steel shim stock. This mask design

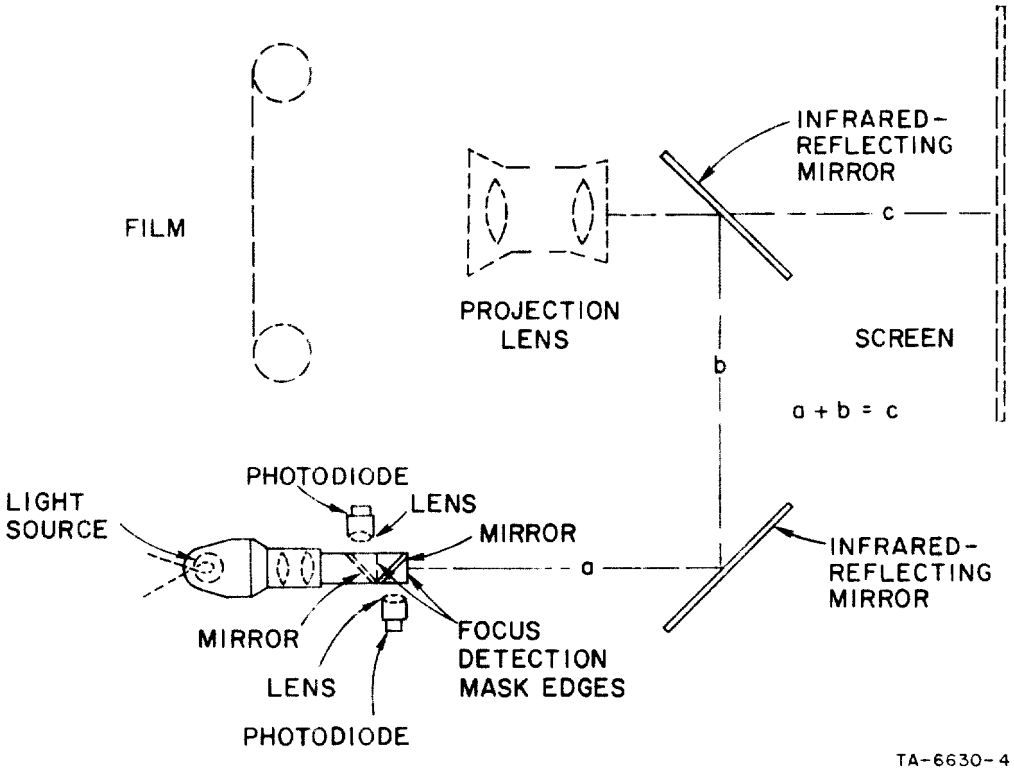

FIG. 4 FOCUS-DETECTION SUBSYSTEM

permits two masks to be staggered along the optical axis in order to provide for a differential output from the two mask photodiodes. In addition, the design allows the use of conventional photodiodes, rather than a combination mask/photocell, which would require specialized photocell development. The arrangement of the focus-detection masks and the detector optics is shown in Fig. 5. A photograph of this assembly is shown in Fig. 6.

When a mask edge is located at an optical distance from the film equal to the film-to-screen distance (via the mirrors--see Fig. 4) and the projection lens is properly positioned, the film image is in focus on the screen and the illuminated image of the mask edge is in focus on the film. This image is reflected by the film surface and is returned back upon the edge itself. Thus, all the light returns on one side of the edge to the source and no light is returned past the other side of the edge. When the projection lens or the film move from

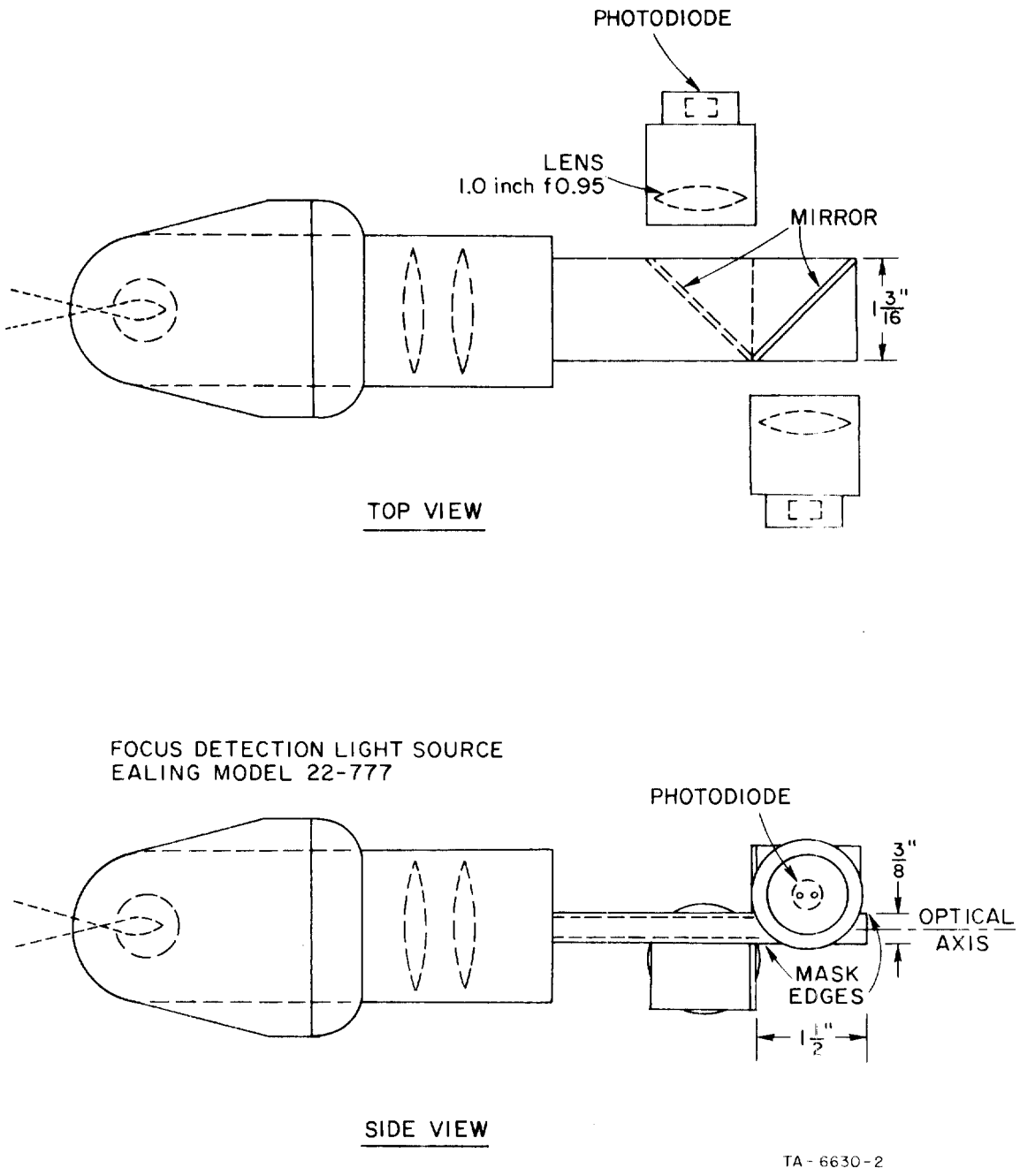

FIG. 5 LAYOUT OF FOCUS-DETECTION MASKS AND OPTICS

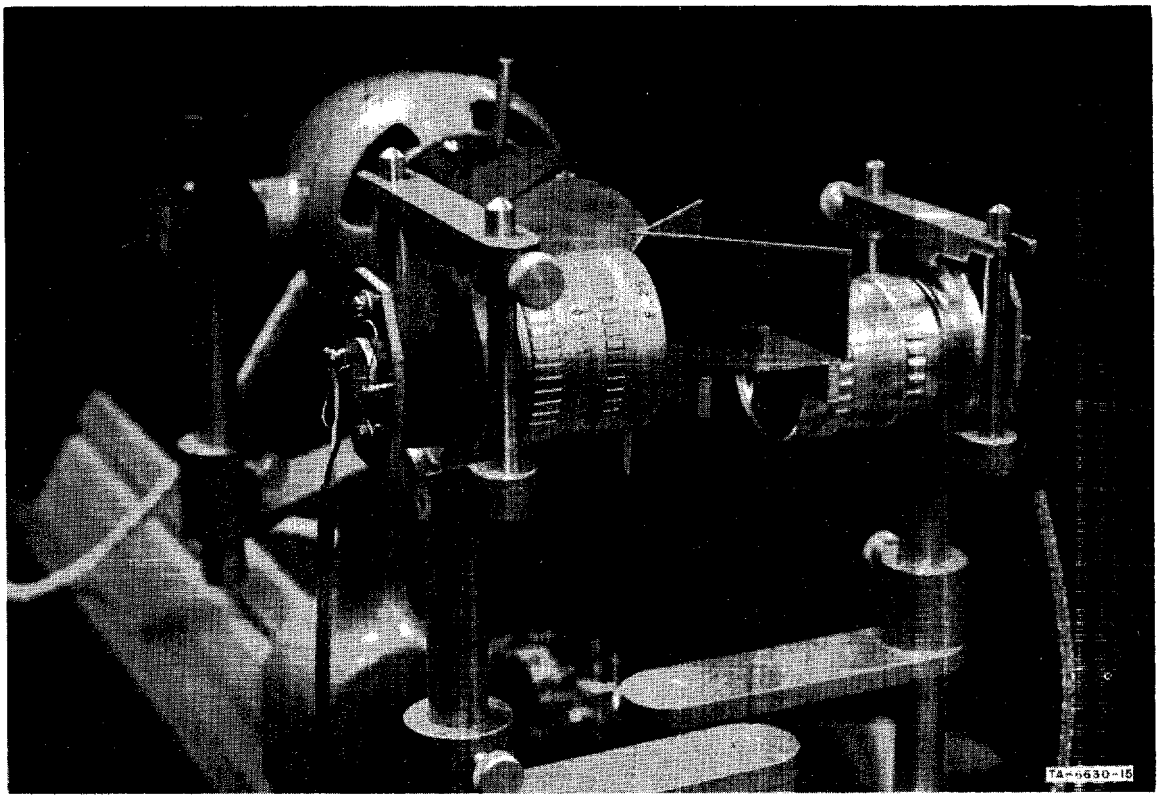

FIG. 6 FOCUS-DETECTION MASKS AND OPTICS

their relative position required for correct focus, the image of the edge of the mask is not in focus on the film and the reflected image back at the mask is out of focus. This results in some light returning on the other side of the mask edge. Light so returned is reflected by the mirror and focused by the collection lens onto the photodiode. Photodiode output as a function of film position as the film plane is continuously moved through focus is shown in the upper trace of Fig. 7, in which photodiode output has been amplified by a high-input impedance operational amplifier with a voltage gain of two.

Because of the symmetry of the signal polarity on either side of focus, it is not possible in a simple manner (using a single photodiode) to determine which side of focus the film has moved. Therefore, two mask edges are used, displaced 1-1/2 inches from each other and

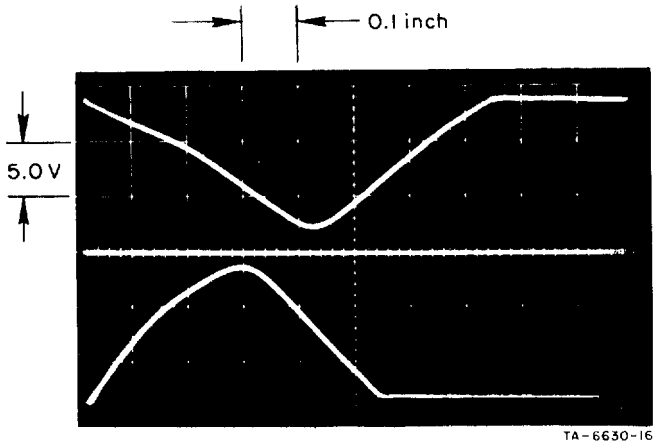

FIG. 7 OUTPUT OF FOCUS-DETECTION DIODES AS A FUNCTION OF LENS POSITION

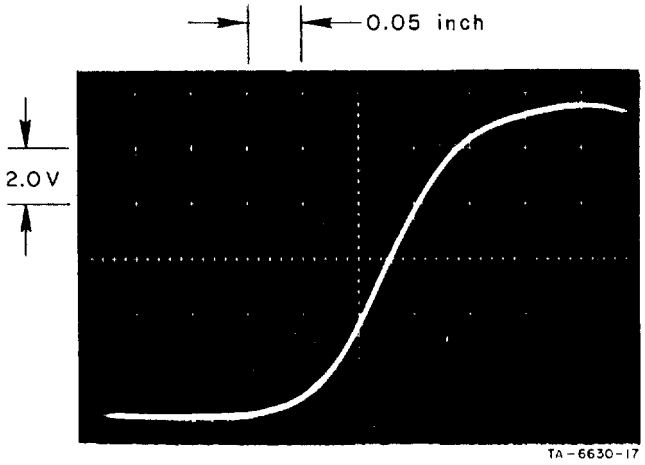

FIG. 8 SUMMED OUTPUT OF TWO FOCUS-DETECTION PHOTODIODES

located on either side of focus.* The lower trace of Fig. 7 shows the output of the second photodiode operated from a negative voltage in order to give an output of negative polarity. The equivalent screen position is approximately midway between the two masks. The exact screen position for precise focus is determined by the zero crossing of the summed output (Fig. 8) of the two curves shown in Fig. 7.

The controlled linear film plane movement used to obtain Figs. 6 and 7 was accomplished by removing the projection light source and film drive and substituting a piece of film that could be moved through the film plane. For small motions, the movement of the projected image along the optical axis is related to the motion of the film by the square of the magnification. Since the mask location corresponds to the screen or image side of the optical system, the 1.5-inch separation of the mask edges correspond to $1.5/m^2$ inches of film plane movement. The exact value of m for the demonstration projector is m = 3.5. Therefore, $1.5/(3.5)^2$. 0.12 inch. This is confirmed by the relative displacement of the null points of the top and bottom traces of Fig. 6. The summation of the two curves, as shown in Fig. 7, provides the required nonambiguous error signal for use as an input to the lens servo subsystem.

The separation distance of the masks was chosen to provide a summation curve with a nearly linear response over a ±0.050-inch range. Preliminary film drive experiments indicated that the peak excursions of the film plane would not exceed this range. By providing an error voltage linear with the focus error, design and testing of the lens servo were kept straightforward.

The selected mask spacing for 3X magnification thus provides a high linear sensitivity over the normal expected operating range of film movements, yet provides an error signal of sufficient magnitude to drive the servo motor and of correct error polarity for a transient error of several times the nominal ±0.050-inch error signal.

---

*A more detailed discussion of both the single and double mask focus detection technique is given in Sec. IV-B.

The circuit used for the two photodiodes is shown in Fig. 9. Under zero-light conditions, the potentiometer R is adjusted to balance the output to zero. Because of the low light levels and the use of each photodiode as the load resistor for the other, the output impedance of the circuit is very high. An operational amplifier is used for the following stage to obtain a very high (>100 MΩ) input impedance and a voltage gain of approximately two. A load resistor was used to lower the circuit impedance to 10 MΩ to reduce the effects of changes in the very high circuit impedance levels upon the circuit gain and to reduce 60 c/s pickup. The output traces shown in Figs. 7 and 8 were taken from the output of this amplifier.

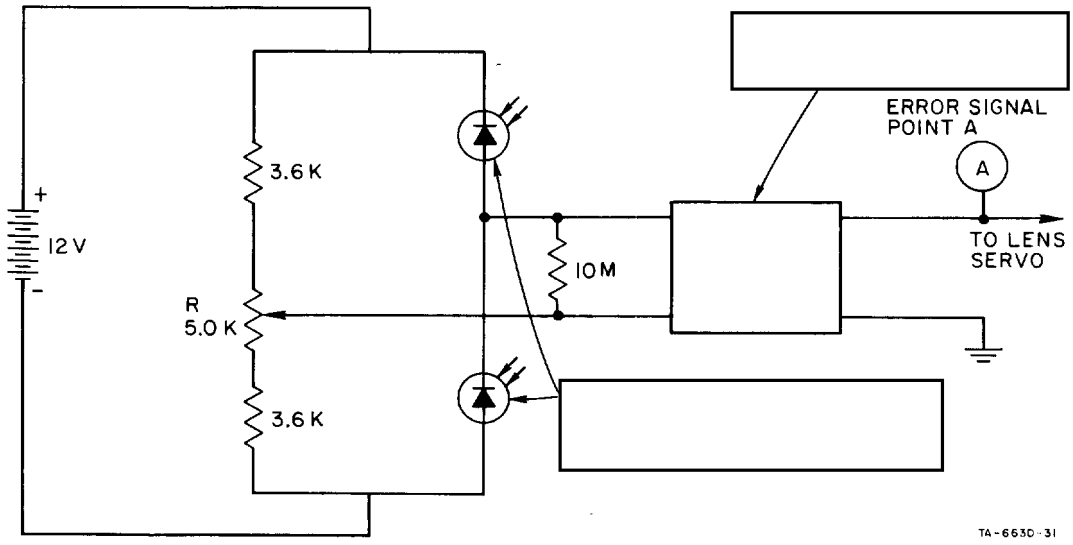

FIG. 9 CIRCUITRY FOR FOCUS-DETECTION PHOTODIODES

A single-mask technique described in the previous project report[1] was considered for use in the demonstration projector, but was rejected in favor of the two-mask approach for three reasons:

(1) The single-mask technique would be considerably more complicated than the two-mask method, even in its simplest form for 3× magnification.

(2) The single-mask technique using a pellicle mirror was known to be feasible from previous work; while it was judged suitable for further experimental application, its reliability for extension to operational applications and environments is questionable.

(3) The simplicity of the two-mask approach was in line with the basic goal of achieving a complete working projector first, and then refining the subsystems with the time and effort remaining after successful 3X scanning operation was achieved.

Following successful operation of the system at 3X magnification, the remaining effort was spent exploring and evaluating the realizable screen resolution during the scanning mode at 3X and in exploring two alternate methods for obtaining higher magnifications.

2. Definition and Interpretation of Focus-Detection Error Signal

The detector mask measures the defocus in the screen image plane, and the error signal is referenced to this plane. When the lens servo is not operating, the error signals can be transformed to give actual film plane motion by the m^2 relationship for small axial displacements of an object and the resultant image displacement. The basic error calibration curve was obtained without the lens servo operating by using a calibrated linear film motion.

Throughout this report, the focus error is usually given in dimensions referenced to the film plane side of the optical system. However, when the lens servo is operating, the error signals represent the error in lens-to-film distance from that required to place the image in focus as defined by the focus-detection mask (or masks) which are located at a fixed position equivalent to the screen. Therefore, when the lens servo is operating, the error signals at frequencies

significantly above the 2 c/s lens servo response represent actual film movement as would be measured from a stationary reference, since the lens does not respond. However, at very low frequencies and at dc, the film movements are compensated for by the lens movement. Therefore, the lens/film combination can together make significant low-frequency movements or steady-state shifts with respect to a fixed reference. These movements are not indicated in the error signal, and do not result in axial image motion about the screen plane. The error signal does, however, give for all frequencies the error in lens-to-film distance required to place the image at the screen plane. This error and the screen image position error are related by the m^2 relationship.

E. Overall Layout

The overall layout of the demonstration model projector is shown in Fig. 10.

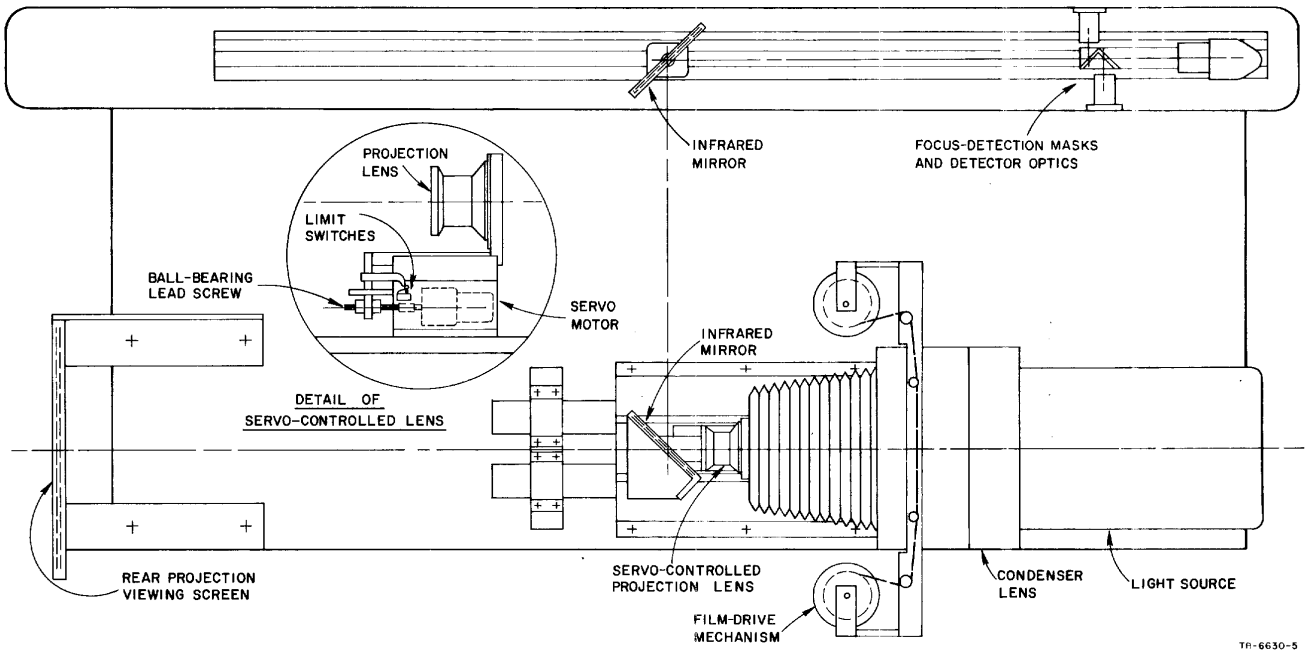

FIG. 10 OVERALL LAYOUT OF DEMONSTRATION REAR-SCREEN PROJECTOR

III BASIC SUBSYSTEM PROBLEMS RESULTING FROM SYSTEM INTEGRATION

A description and explanation of the performance achieved with the demonstration rear-screen projector must, of necessity, be presented in the light of problems resulting from system integration. Accordingly, this section on system integration problems precedes the section devoted to performance of the demonstration projector.

A. Light Reflections Degrading the Performance of the Focus-Detection Subsystem

The operation of the focus-detection system is based on the precise reimaging of a mask image back upon the original mask. Accordingly, light entering the detector area from any source other than reflection from the front film surface is detected as defocused light. The result is reduced sharpness, modified shape, and shifted position of the null voltage characteristic of the photodiode indicating focus for that mask.

Significant sources of undesired light are treated in the following paragraphs.

1. Light from the Projection Light Source

Light from the projection light source is successfully eliminated by spectral filtering. The focus-detection system is operated at infrared wavelengths longer than 7000 Å. A Wratten No. 88A filter is placed in front of the photodiodes and an infrared absorbing glass filter with a dielectric film coating to reflect wavelengths longer than 6800 Å is placed in the output of the main projection light source. This permits only visible light to illuminate the film for the projected image. The mirrors used in the focus-detection system are deposited film mirrors, which reflect infrared and transmit visible light. (These mirrors permit some reflection in the deep red end of the visible spectrum, allowing visual inspection of the focus-detection image on the film for alignment and for experimental observation of the functioning of the focus-detection subsystem.)

With the filtering system used in the demonstration projector, there has been no measurable effect of the 300 W light source upon the output signals from the photodiodes. The photodiodes used as detectors have a peak response at 1 μ; therefore, the spectral passband represented by the Wratten No. 88A filters could be shifted to slightly longer wavelengths and, if needed, replaced by sharper cutoff deposited-film filters without significant effect on the photodiode sensitivity.

2. Light from the Focus-Detection Mask Reflected from Objects Other than Front Surface of the Film

There are three significant sources of reflections from objects other than the front surface of the film.

a. Light Reflection from Components Behind the Film

Spectral reflection from the film used for focus detection has been determined to be about 3 to 6 percent of the incident intensity. In clear areas of the film, the absorbtion of the transmitted light amounts to only a few percent. Therefore, about 90 percent of the focus-detection image passes through the clear film areas for subsequent reflection by any surface encountered. The condenser lenses in the projector light source are normally placed a short distance behind the film. In the STAT lighthouse used in the demonstration model, the condenser system consists of two plano-convex lenses, placed convex-side inward. Thus, the plane surface of one condenser is directly behind the film--in the demonstration model approximately 1/2 inch away from the film. The result was a significant reflection of the focus-detection image from the front and successive surfaces of the condenser lenses. Since the condenser lenses are not low-reflection coated, the reflection from the front surface was of the same magnitude as that from the film when clear areas permitted over 90 percent of the focus-detection image to reach the condenser lens surface. This out-of-focus reflection varies in intensity with film image density in the central spot used for focus-detection reflection. The result is a large, film-image-modulated reflection, completely masking the minimum defocus light being returned from the film at the desired in-focus film position.

While coating of the condenser lenses would have reduced the reflection, a simpler and more effective solution was employed. A 5/8-inch square wedge of infrared-absorbing glass was attached to the center of the surface of the condenser lens directly behind the film in the area through which the focus-detection image would pass and encounter the condenser lens (see Fig. 11). Light from the focus-detection image passing through the film is reflected at such an angle as to miss the projection lens on its return.

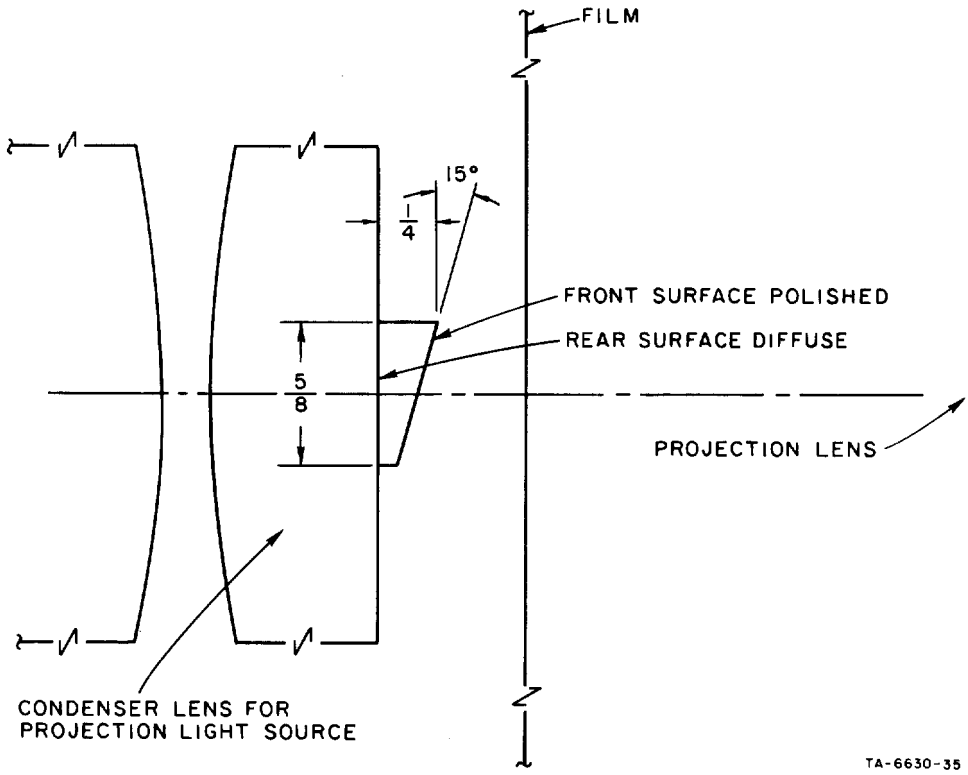

FIG. 11 TECHNIQUE USED TO ELIMINATE SPURIOUS FOCUS-ERROR SIGNAL FROM CONDENSER LENS

If this front-angled surface were coated with the same film employed on the mirrors used in the optical path of the focus-detection subsystem, essentially the entire focus-detection image transmitted at infrared wavelengths would be diverted by the wedge; other surfaces of the condenser lens system would thus receive no light to

reflect. The visual light from the projection source would pass, unattenuated, to the screen image for viewing. Therefore, coating this surface is recommended in future models.

A satisfactory interim solution was achieved by making the second surface of the wedge a diffusing surface; this was achieved by sandblasting with a very fine sand. The nearly spherical distribution of reflected light from this surface (compared to the small solid angles subtended by the projection lens) reduced the reflection to a nondisturbing level in the demonstration projector.

The diffuse rear surface of the wedge was employed for a second, unrelated reason. The diffuse-surface was needed for the demonstration and evaluation of the concept of leaving a clear area in the center of the screen where part of the projected image can be examined with a magnifying lens. It has been found desirable to provide a diffuse illumination of that portion of the film; the diffuse rear surface of the wedge serves that function. Detailed discussion of the technique of using an auxiliary magnifier for higher magnification is presented in Sec. IV-B-2.

b. Light Reflection from Mirrors and Mechanical Components in the Focus Subsystem Optical Path

The minimization of the illumination of nonoptical components from the mask aperture source and the careful coating of all such objects with flat-back paint satisfactorily reduced reflections from these components. However, this potential problem area would require careful attention during construction of a prototype model in a closed cabinet. Careful confinement of the mask illumination beam from the focus-detection light source (prior to illumination of the mask edge) to a cone just covering the front element of the projection lens would be desirable to minimize stray reflections from other components.

The front-surface infrared-reflecting mirrors are an unavoidable source of some stray reflections. Low-reflectance coating of the second surface and provision for minimizing and cleaning dust accumulation from the front surface are small but significant considerations.

c. Light Reflections from Rear Surface of the Film

Film is loaded in the projector with the emulsion side away from the projection lens. Three interface boundaries are encountered by the focus detection light pattern. The first of these is at the front surface of the film support material. The specular reflection from this surface is, of course, desired for the focus-detection reflection.

A second interface surface is the boundary between the film base and the emulsion layer. Any reflection from this interface (due to differences in index of refraction of the two film base and gelatin) is assumed to be small (or at least constant) and unaffected by the silver layer in the gelatin.

The third surface is the gelatin-to-air interface at the back side of the film. Late in this project, it was discovered that a significant reflection occurs from this surface and, because of the density variation of the silver layer forming the image in the gelatin, the magnitude of the reflection is modulated by the image. This modulation by the moving image, coupled with the high sensitivity of the two-mask focus detection technique to differences in reflected light level between the two masks, lead to the discovery and measurement of this significant source of reflection. Comparative measurement of the total reflected light from the focus-detection image for clear and dense black film areas indicate that, in clear areas, the rear-surface reflection is nearly equal to the front-surface reflection. Thus, the effect on the focus-detection system is a maximum for clear film. The resulting focus-detection error caused by clear-area reflection is different for single- and dual-mask focus-detection techniques.

Assume that the rear-surface reflection is equal in magnitude to the front-surface reflection. For a single mask, the ideal focus detection curve for a single surface reflection would have a single notch, as shown in Fig. 12(a). The added notch and curve for the second surface is shown dotted in Fig. 12(b), and its null is displaced by the film thickness. The summation of the two nulls shown in

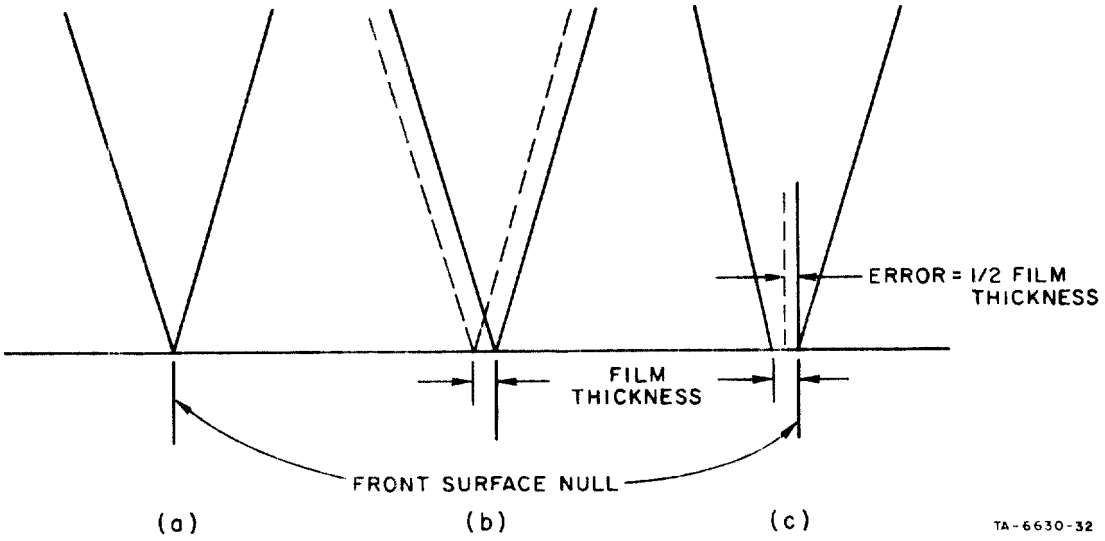

FIG. 12 FOCUS ERROR FOR SINGLE-MASK TECHNIQUE DUE TO REAR-FILM-SURFACE REFLECTION

Fig. 12(c) is the resultant output curve. The center of the resultant null is located at a point one-half the film thickness behind the original front surface null location. Thus, the error range for a single mask can vary from zero to one-half the film thickness.

For the dual-mask technique, the above error applies to each mask. If the two masks were reflected from the same area of the film (or made to alternately reflect from the same areas at a rate sufficiently higher than the desired lens servo response frequency), the net error for the two-mask system would also be one-half the film thickness. However, if different areas are constantly used for the mask reflections, the zero point of the summed mask null curves can shift by an amount considerably larger than the film thickness. Figure 13 shows the idealized mask nulls and the summation curves for equal and unequal (2:1) mask reflections.

Simple geometric analysis of the idealized mask curves show that the shift in the zero crossing is 1/6 the mask separation ψ in the direction of the clear-area reflection for the assumed worst case, i.e., where one mask has a rear-surface reflection equal to the front-surface reflection.

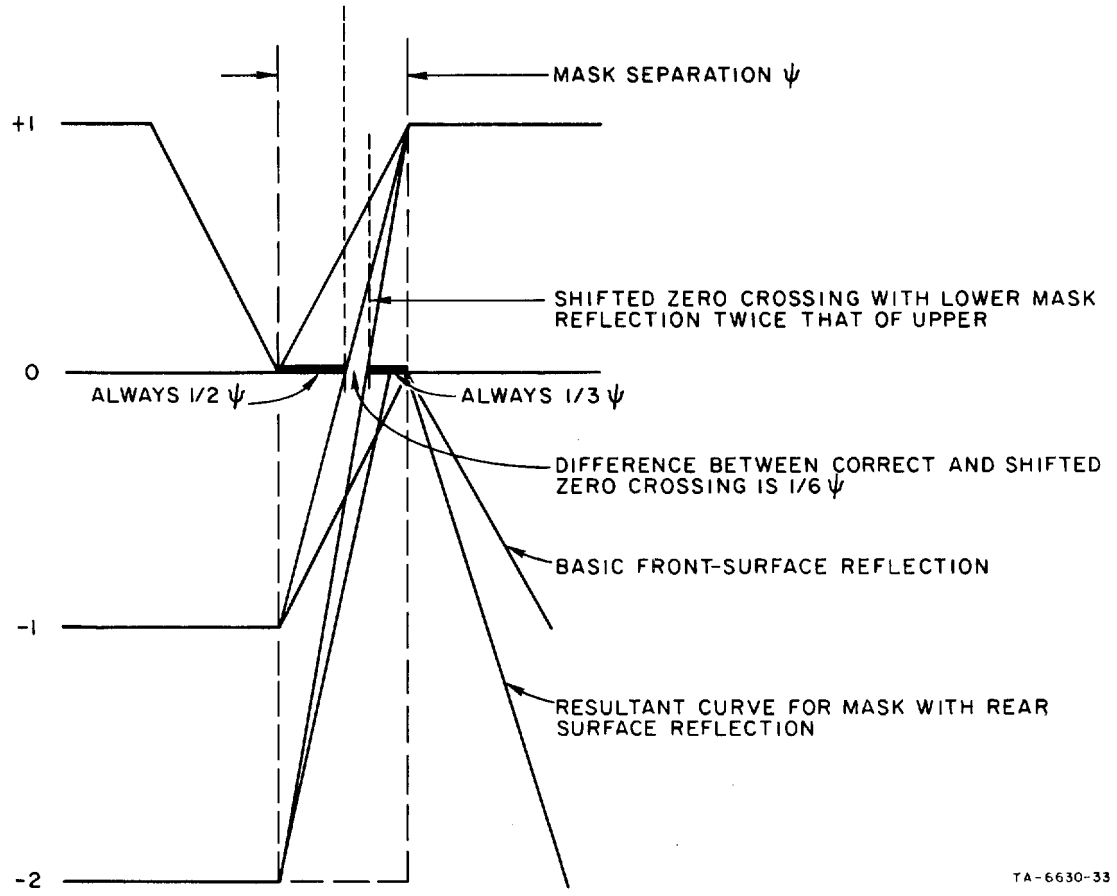

FIG. 13 FOCUS ERROR FOR DUAL-MASK TECHNIQUE DUE TO REAR-FILM-SURFACE REFLECTION

For the demonstration projector, the mask null spacing ψ, is 0.120 inch in the film plane. Since either mask can be the one with a clear-area reflection, the error signal can be $\pm(0.120/6) = \pm 0.020$ inch maximum. False focus error fluctuations approaching this value are observed in the demonstration projector.

Two suggested techniques for reducing this error for the dual-mask focus detection technique are:

(1) Use a beam splitter to measure a known proportion of the total light returned from each mask image. Using this information, the gain of an amplifier

could be controlled over the 2:1 range required to make the null curve from each mask a constant slope and thus independent of the magnitude of the second-surface reflection. The resultant error in the focus detection position would be reduced from 1/6 ψ to half the film thickness.

(2) Design the focus-detection subsystem so that the image on the film for each mask occupies the same area or are made to rapidly move about in a suitable manner such that each image scans the same film areas. This would again reduce the error to half the film thickness.

Reduction of the basic error of half the film thickness for each mask would require a refinement of technique (1). In addition to modifying the gain for the slope of the null, an additional input voltage to the lens servo summing point could be generated that would shift the lens position from the indicated null by an amount proportional to the measured rear-surface reflection. For a rear-surface reflection equal to that from the front surface, the shift would be half the film thickness.

B. Film Vibrations

The major sources of film plane motions are the specific characteristics of the film transport subsystem and the external mechanical and pneumatic sources of excitation that can be coupled to the film. The significant components that determine the film plane motion characteristics are the film guides, the film tension, the presence of a rear-glass platen, a clamping platen, and the spacings of the film and platen during film scanning motion.

The effect of external excitations (from other subsystems and the outside environment) on the film motion will depend on the following factors:

(1) Resonant frequencies of the film as determined by film base characteristics and film drive tension.

(2) Damping characteristics provided by the air film or air spaces surrounding the film. Care must be taken in the design and use of such air damping to ensure that unwanted mechanical or pneumatic inputs to these chambers do not cause film plane motions.

(3) Mechanical isolation of the film drive from the remaining structures, in particular from the lens servo subsystem.

(4) Proper venting of the projection lens bellows system to prevent air coupling between the servo-controlled movements of the projection lens and the film.

It is important to minimize the film plane curvature since automatic focus can only place one plane in critical focus. High-frequency vibration about the exact focus plane causes less degradation in image resolution than a fixed error. This is discussed in Part C, following.

C. Observable Screen Image Resolution with Film Plane Oscillation

The visual appearance of the image on the screen during scanning at 3X magnification was that of a sharply focused image, although sharpness of the image could not be established quantitatively under the conditions, since the image was in motion corresponding to the 2 inch scanning speed of the film. A separate experiment was designed to permit a quantitative measure of the effective resolution on the screen at 3X magnification with the film oscillating about a median focus at magnitudes and frequencies similar to those expected for the film drive for the demonstration projector. The equipment for this experiment is shown in Fig. 14.

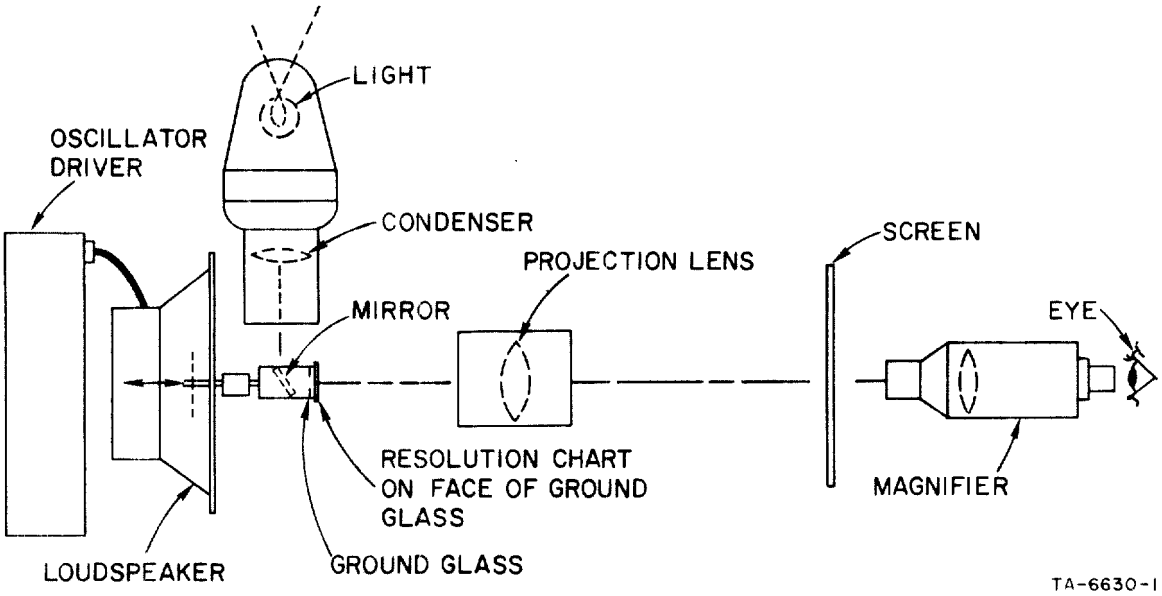

FIG. 14 LABORATORY SETUP FOR DETERMINATION OF SCREEN IMAGE RESOLUTION WITH AXIAL FILM PLANE VIBRATION

A loudspeaker was used as an electrical-to-mechanical transducer to provide a controlled frequency and amplitude mechanical motion of an illuminated film resolution chart. Figure 15 shows the illuminated film resolution chart and the speaker drive unit. The resolution chart is imaged by the same projection lens used for the 3X magnification on the demonstration projector. The image is focused on a piece of standard rear-screen projection material. The image was examined through a high-quality, extra-wide-field eyepiece used as a 7X magnifier. With the resolution chart stationary and the system critically focused, resolution bars representing 50 lines/mm on the film or $50/3 \approx 17$ lines/mm on the screen surface were clearly distinguishable. A steady-state displacement of ±0.064 (1/16) inch in either direction from critical focus reduced the distinguishable resolution at the screen to 4 lines/mm for the resolution of the screen image. The normal unaided eye can resolve about 10 lines/mm at the normal close viewing distance of 10 inches. Therefore, a screen resolution of 10 lines/mm would ensure that the eye is the limiting factor during the normal 15 to 20 inch viewing distance used for the 3X scanning mode.

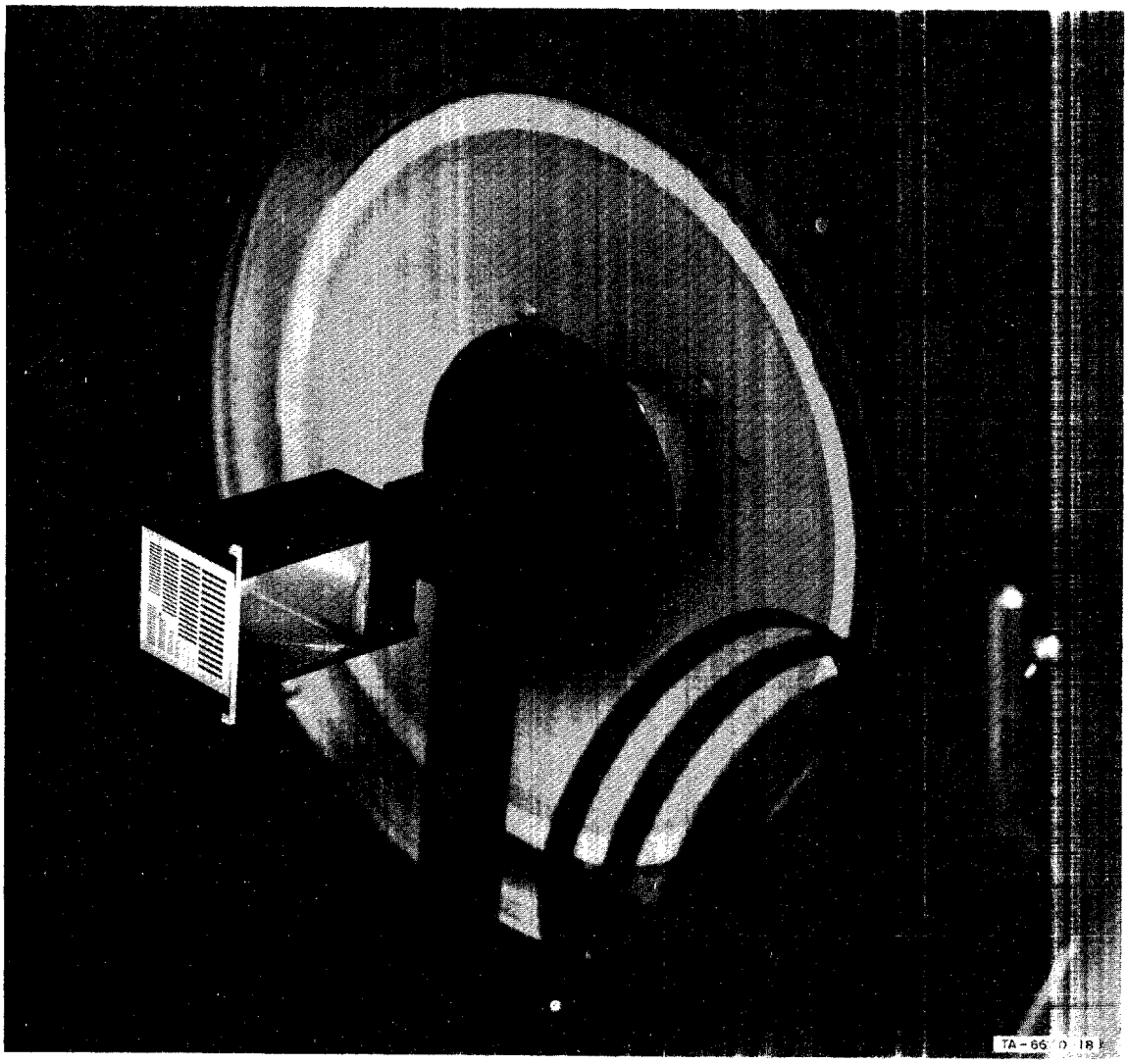

FIG. 15 RESOLUTION CHART AND AXIAL VIBRATION DRIVER

The significant result of this test is that it is not necessary to design the lens servo system for high-frequency response. A low-frequency response with as high as possible dc gain will maintain an average focus about which the high-frequency vibration of the film can occur without causing a serious loss in resolution.

IV PERFORMANCE OF THE DEMONSTRATION REAR-SCREEN PROJECTOR

A. System Performance at the Basic Scanning Magnification of 3X

1. Performance Measurement Technique

The measured performance of the focus-detection and lens servo systems under various operating conditions are shown in a series of oscilloscope photographs of the error signal voltage from the focus detector amplifier.* This error signal voltage is related to the deviation from the correct lens-to-film distance by the focus detection curve (Fig. 8). This curve is nearly linear for lens-to-film distance errors less than ±0.050 inch with corresponding output error voltages of less than ±4.0 V. The error voltage sensitivity is 80 V/in; this value is used in the following evaluation of focus performance, since all recorded error voltages are less than ±4 V. The oscilloscope photographs presented here were taken with the operational demonstration projector. Servo gain was set at the optimum value, as described in Appendix A.

2. Performance with Film Stationary

Figure 16 shows the error signal with the film stationary. At a scope sweep speed of 5 s/div, a 50-s period is displayed. The average peak-to-peak error signal is slightly less than ±0.1 V, corresponding to ±0.001-inch error in the film-to-lens distance for exact focus. Figure 17 shows an expanded trace covering a 1-s period.

These representative pictures show that the major error voltage excursions occur at frequencies of 10 c/s and above. The low-frequency variations (below 2 c/s) and the average value are one-half to one-third smaller than the peak-to-peak excursions of the error signal. This is to be expected from the servo specifications (Appendix A) and the measured dc gain, for which a focus error of 0.0002 inch

*The same signal used for Figs. 7 and 8 of Sec. II; measured at Signal Point A shown in Fig. A-3 of Appendix A.

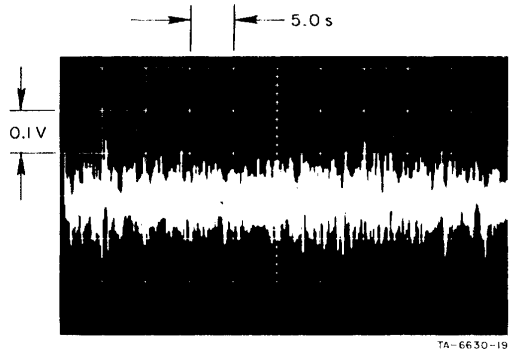

FIG. 16 FOCUS-ERROR SIGNAL FOR STATIONARY FILM — 50-S SWEEP TIME

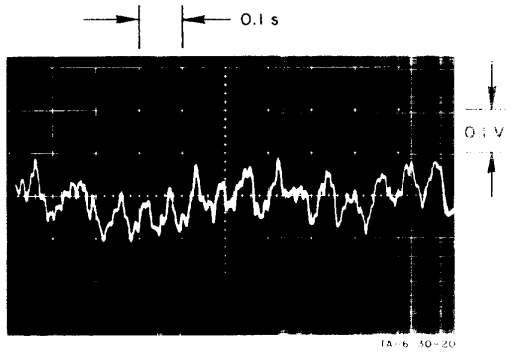

FIG. 17 FOCUS-ERROR SIGNAL FOR STATIONARY FILM — 1-S SWEEP TIME

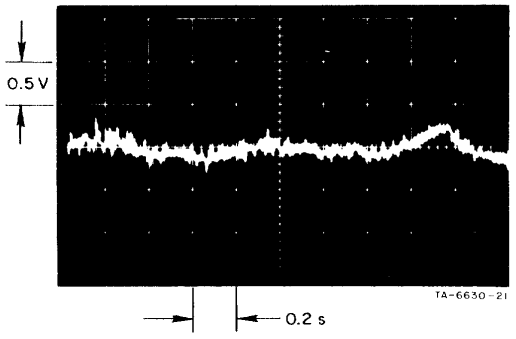

FIG. 18 FOCUS-ERROR SIGNAL FOR FILM MOVING AT 2 IN/S — 2-S SWEEP TIME

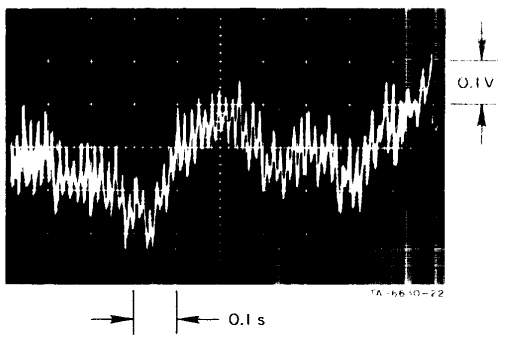

FIG. 19 FOCUS-ERROR SIGNAL FOR FILM MOVING AT 2 IN/S — 1-S SWEEP TIME

would generate an amplified voltage equal to the breakaway voltage required by the servo motor. The lens servo bandwidth was reduced to 2 c/s from the design value of 5 c/s to prevent oscillation that might otherwise result from mechanical feedback coupling between the lens servo and the film. (This instability resulted in a 40 c/s oscillation of the servo system when the desired dc gain was used with the designed servo bandwidth of 5 c/s.)

3. Performance at Scanning Speed

Figures 18 through 21 show the performance of the system with the film in motion at a scanning speed of 2 in/s. Figure 18 shows a 2.0-s oscilloscope trace with a steady film speed of 2 in/s. Figure 19 shows scope trace covering 1.0 s with higher vertical gain at the same 2.0 in/s film speed. These representative samples show that the error signal reaches ±0.3 V on occasion; a more typical value ranges between 0.1 to 0.2 V. From the calibration factor of 80 V/in, this error signal would indicate a relative lens-to-film distance error from the correct focus distance to a maximum value of ±0.004 inch with a typical excursion of ±0.002 inch. The predominant high-frequency signal is 60 c/s pickup from the photodiode amplifier circuitry.

Figures 20 and 21 show the difference in performance with the servo operating and not operating as the film drive is intermittently stopped and run at 2 inches per second. In Fig. 20, the servo is operating while the film drive starts and stops for 2-s periods during the 10-s period covered by the recording trace. The error signal amplitudes are similar to those shown earlier for both running and stopped conditions, except for a transient error at the leading edge of each 2-s period of film motion. The average value of all the stopped periods, however, can be seen to be the same. Figure 21 was taken with the servo disabled. The different stationary positions of the film are quite apparent.

Figures 20 and 21 indicate a difference in successive stopping positions without the servo operating represented by a 1.5 V error signal, corresponding to 0.019 inch. This variation is outside the depth

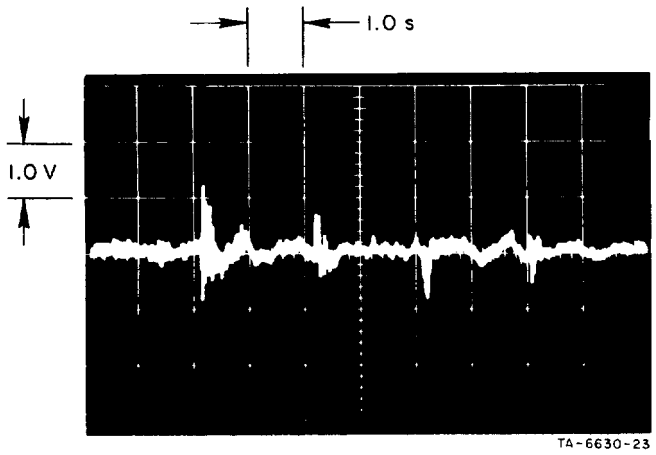

FIG. 20 FOCUS-ERROR SIGNAL WITH SERVO OPERATING, FILM ALTERNATELY STARTING AND STOPPING AT 2-S INTERVALS

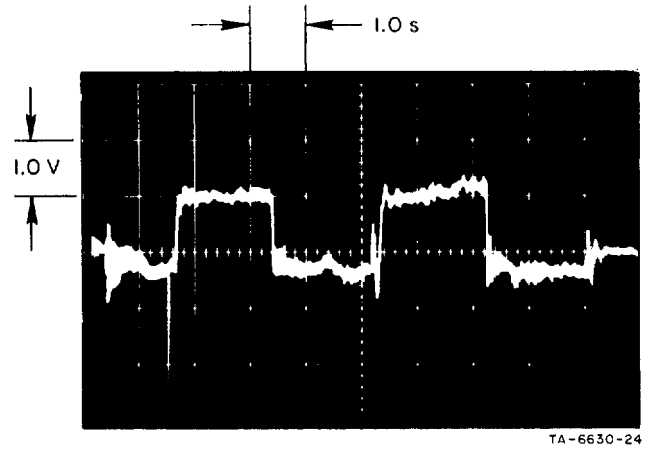

FIG. 21 FOCUS-ERROR SIGNAL WITH SERVO DISABLED, FILM ALTERNATELY STARTING AND STOPPING AT 2-S INTERVALS

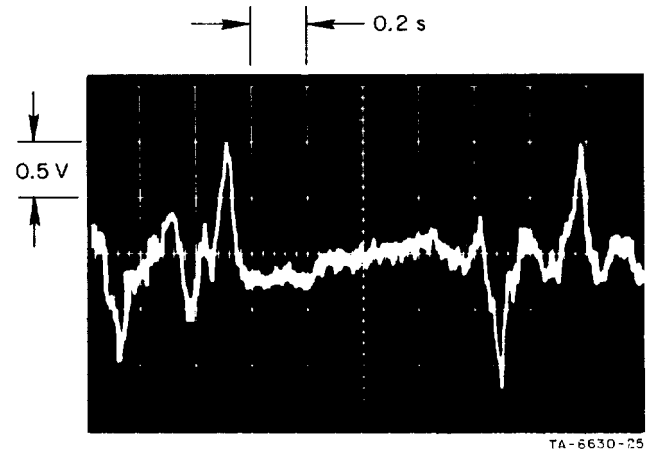

FIG. 22 EFFECT OF REAR-FILM-SURFACE REFLECTION

of field of the optical system at 3X magnification and results in reduced screen resolution. The depth of field curves presented in Fig. I-19 in the previous project report[1] indicate that the acceptable error in lens-to-film distance for a screen resolution of 10 lines/mm with an f 5.6 lens and a 3.5X magnification is ±0.006 inch.

The measured results presented in Figs. 18 and 19 indicate peak errors within this range. The oscilloscope photographs from which the focus-error data were taken were made using a section of film of a uniform density and no image pattern. (The use of film with uniform density eliminates the small false error signals found to exist when normal image patterns are used. This source of signals was described in detail in Sec. II-A-2-c.)

4. Effects of Reflections from Rear Surface of Film

The effect of the rear-surface reflection is shown in Fig. 22, where the center four divisions of the recorded error signal represent the passage of a 1.6-inch length of dark uniform film area. In the areas outside the center four divisions, the error signal is larger and contains a succession of sharp positive and negative error signals with amplitudes indicating focus errors of 0.010 to 0.015 inch. These indicated focus errors are caused by the image-modulated rear-surface reflections described in Sec. II-A-2-c and not from film plane motions. When the film is moving, image patterns normally cause variations in the rear-surface reflections at frequencies above the 2 c/s servo response, which thus are not compensated for by the servo. Pattern variations changing slowly over large film areas or with stationary film can produce false error signals below 2 c/s to which the servo can respond. Thus, the lens servo can cause the system to go out of focus on the basis of a false error signal. Since the maximum error that can be produced in this way is ±0.020 inch, the performance of the demonstration model is limited by this error.

As described in Sec. III-A-2-c, the false error signal can be reduced or eliminated by refinement of the focus-detection subsystem. The focus detection sensitivity and lens servo performance under static

film conditions are not the limiting factors in achieving the accuracy in the present system or the accuracy that could be achieved for a refined focus-detection subsystem. It is the inability of the focus-detection subsystem to identify the correct film surface that limits the overall focus performance at 3X and its extension to higher magnifications. Accordingly, in summing up the performance of the demonstration projector, two sets of figures will be given. One set represents potential performance if the outlined (but as yet unincorporated) refinements to the focus-detection subsystem were incorporated and proved successful. The second, degraded set of performance figures are based on the worst-case estimate of the present false error signals. Where appropriate, in the following sections that discuss the potential configurations, the requirements, and the problem of extending automatic focus-detection techniques to higher magnifications, the distinction is made between these two sets of data.

5. Summary of Performance at 3X

Focus detection and lens servo subsystems have been successfully operated on the 3X magnification rear-screen projector. The basic problems of subsystem integration have been solved and the complete projector with focus detection and control could be operated at film speeds from 0 to 4 in/s. The sensitivity of focus detection and control was 0.0002 inch of lens-to-film distance focus error. The accuracy of the focus detection was limited to ±0.020 inch by the rear-film-surface reflection.

Several techniques could be used to correct the focus-detection output for the errors introduced by the rear-surface reflection. The incorporation of one of these techniques would reduce the focus detection error to a total range of half the film thickness. Thus, for film that is 0.004 inch thick, the accuracy of the focus detection would be 0.002 inch. An additional refinement was also outlined that could further reduce this error by a factor of 3 to 5.

B. Operation at Magnification Above 3X

There are two basically different ways to provide for higher magnification examination of a portion of the image.

(1) Shorten the focal length of the projector lens, which increases the magnification of the screen image. This can be accomplished by either lens substitution using a selected set of fixed focal lengths or through the use of a variable focal length projection lens. These are the conventional techniques normally used for rear-screen projectors.

(2) Use additional optical components to permit the magnification of a portion of the low-power (3X) screen image. To prevent both a loss in resolution and illumination level due to the screen characteristics, this method requires that a small area of the screen be removed where the image is to be examined at higher magnification.

In the following paragraphs, the advantages and disadvantages of these two approaches are discussed and related to the present focus-detection subsystem.

1. Use of Shorter Focal Length Projection Lenses

The focus-detection techniques studied on the present and preceding project employ two masks and one mask, respectively. In theory, both techniques can be applied to rear-screen projectors with highly magnified screen images; however, as the magnification is increased, the detectable range of film motion is reduced. The degree to which the magnitude of the allowable film plane motions can be reduced is limited by the film drive characteristics. The work on this project has been based on the use of film drives that do not employ glass film platens to constrain the film plane motion.

From the experience with the film drive used on this project, a film excursion of ±0.050 inch has been selected as a minimum value for use in analysis of double- and single-mask focus-detection techniques at high magnification.

a. Double-Mask Focus-Detection Method

The performance of the demonstration rear-screen projector was not measured at high magnifications because of the basic limitation of the two-mask focus detection. This limitation results from the relationship for small motions along the optical axis

$$\frac{\Delta \text{ image motion}}{\Delta \text{ film motion}} \cong m^2 \quad ,$$

where m = image magnification.

If the maximum film excursion is ±0.050 inch, it is reasonable to require that the effective separation of the two masks be equivalent to at least ψ = 0.1 inch (measured in reference to film side of the optical system).* For a magnification of 3X, the actual mask separation would approach $0.1 \times 3^2 = 0.9$ inches; at 10X the separation would approach $0.1 \times (10)^2 = 10$ inches, which is near the practical limit for mask separation. Further increases in m with the masks held at 10 inches will result in a reduction in the effective separation of the masks in the film plane. Thus, for a mask separation of 10 inches and for m = 20, the equivalent mask separation in the film plane (ψ) would be

$$\psi \cong \frac{10}{(20)^2} \cong 0.025 \text{ inch}$$

*The separation of the masks corresponds to the separation of the voltage nulls from the photodiodes as shown in Fig. 1. The summation of the outputs as shown in Fig. 2 gives the basic focus error voltage for input to the lens servo. When the mask separation, referred to the film side of the optical system, is made equal to the expected film excursion range, the resulting focus error voltage has both a suitable linear range and a safety factor for unexpected excursions.

and for m = 70, ψ would reduce to

$$\frac{10}{(70)^2} \cong 0.002 \text{ inch} \quad .$$

Thus, the extension of the two-mask focus detection technique to magnifications somewhat above 10X is feasible if expected film plane excursions can be reduced and by accepting a reduced linear range and safety factor in the relationship between the focus detection curve and the expected film excursion. Extension of the two-mask technique to very high magnifications does not appear feasible.

b. Single-Mask Focus-Detection Technique

The distance separating the nulls of the photodiode output curves for two masks must be clearly differentiated from the width of the null in the output curve for a single mask. A discussion of the shape of the photodiode output curve for circular masks and the relationship of the width of the null to the basic parameters of mask diameter, lens diameter, and magnification is given in detail in Appendix B.

Use of a single-mask null for detecting focus errors requires the use of a technique described in the previous project report,[1] in which a pellicle mirror provides a high frequency (>50 c/s) variation of the focus-detection optical path length, thereby enabling detection of the different slopes of the two sides of the single-mask null curve. Thus, the direction of the focus error can be determined when using only one mask.

In contrast to the m^2 relationship between the mask separation and the null separation in the film plane for the two-mask method, the critical relationship between mask diameter and the null width in the film plane is linear with m. The width of the null (in film plane dimensions) for a single circular mask is shown in Eq. (B-37) in Appendix B to be

$$\Delta q_R = 2 \frac{w}{m} F \quad ; \qquad (1)$$

another important parameter is given by

$$\alpha = \frac{w}{mD} \quad , \tag{2}$$

where α defines the shape of the null curve (see Fig. B-10). In the above equations w is the diameter of a circular mask, m, the image magnification, F, the f-number of the lens, and D is the lens diameter.

An added constraint in the rear-screen projector application is that the film-to-screen distance is held a constant. In order to keep a given Δq_R a constant, based on the maximum film plane excursion expected, and assuming a given lens f-number for all magnifications, the mask diameter must increase linearly with m. The loss of image illumination with increasing magnification could be partially compensated for by using lower f-number lenses as the focal length gets shorter. If this were done, it would modify the assumption of a constant f-number and mean that w would increase somewhat greater than linearly with m.

The implications of these relationships for three magnifications are shown in Table II and are computed based on the following assumptions. The quantity α will be required to be <0.1 as a reasonable upper limit selected by reference to Fig. B-10. (The lowering of the right side of the null curve with increasing values of α restrict the choice of α to a maximum of 0.1.) A minimum film excursion range of 0.1 inch will be used and hence a value of Δq_R equal to 0.1 will be assumed. A lens-to-film distance of 65 inches, equal to that used on the demonstration projector, will be used. The formula given for Δq_R is based on the assumption that the lens-to-film distance is equal to the lens focal length. This is a good approximation for magnifications above 10. The error in w at m = 3 is less than 25 percent and is insignificant for the present comparisons.

The mask diameters shown in Table II are easily realizable; however, there are several problem areas associated with the implementation of a system using the larger mask diameters required for high magnification.

Table II

MASK APERTURES REQUIRED FOR SELECTED MAGNIFICATIONS

Δq_R (inch)	m	Lens f-Number	Required Mask Aperture (inch)	α
0.1	3	4.0	0.04	0.005
0.1	20	4.0	0.25	0.016
0.1	70	4.0	0.9	0.07

(1) The collection area required for the defocused light from the returned mask image must cover an area from the mask radius r out to a radius $>5r^*$ in order to maintain the desired Δq_R null width. As the mask apertures are enlarged, the resulting large collection areas become more difficult to implement.

(2) The diameter of the optical path required between the lens aperture and the large ($\approx$5 inch at 70X with $\Delta q_R = 0.1$) diameter of the collection area required for the higher magnifications would make difficult the introduction of the pellicle mirror and associated optics required to achieve the optical path variations needed for the single-mask focus-detection system.

(3) As a result of maintaining the required null width Δq_R, dictated by the assumed film plane variations, the slopes of the

*The derivation of the collection area diameter required for the defocus range Δq_R as a function of α and w is given in Appendix C.

basic null curve remains constant. This is derived in Appendix D. However, the allowable error in focus is decreasing as m increases. Thus the null point in the focus-detection curve must be detected more accurately as m increases. Two factors combine to reduce the sharpness of the null and hence degrade the accuracy of null detection. The diameter of mask aperture increases with m; hence, the area and resultant light flux through the mask aperture is increasing as m^2. The light collection diameter surrounding the mask aperture is also increasing with m and its area as m^2. As discussed in detail in Sec. II-A, stray reflected light from the mask aperture illumination is detected by the photodiode as defocused light from the mask image. The main effect of such stray light is to mask the null voltage and reduce the detection sensitivity around the null. The detected stray light is thus increasing as $(m)^4$, and will have serious effect on the sensitivity and accuracy with which the null can be detected. Reduction of the stray light will be a most difficult practical problem to overcome in applying the single-mask focus detection to high magnifications.

The primary advantage of using a magnified screen image results with an assumed desirability of not requiring the operator to

change his mode of viewing (i.e., an unaided binocular view of the screen at distances of 1 to 4 ft) as the magnification of the image is changed.

The major disadvantages of this technique are

(1) The complexity and cost of a rear-screen projector capable of a wide range of screen magnifications will be significantly greater than a projector with a fixed low-power magnification, but with provision for higher magnification examination of a portion of the screen image. The increased complexity results not only from the additional projection lenses required or the use of a variable focal length (zoom) lens, but in the increased complexity of the film illumination source in order or provide suitable screen illumination at high magnifications.

(2) Maintaining image resolution at high magnification imposes tolerances on film plane positioning (with or without automatic focus detection) and upon both the resolution and flatness of field capability of the projection optics that is difficult and costly to achieve.

2. Use of Auxiliary Optics to Magnify a Portion of the Image

The basic projector would have a fixed (3×) magnification of the 9 × 9-inch film frame to provide a 27 × 27-inch screen image. A focus-detection subsystem using the simple two-mask method could be

used. A section of the screen approximately 2 inches in diameter would be removed from the center of the screen and a magnifier mounted to permit a magnified examination of the real 3X image projected in the plane of the screen. The basic layout is shown in Fig. 23. This area should be in the center of the screen and on the optical axis of the projection lens for two basic reasons. Since the focus-detection subsystem is making its measurement on the optical axis, the lens servo subsystem maintains the optimum focus for the central image. Additionally, the main projection lens provides its best resolution of the image in the center of its field, i.e., along the optical axis.

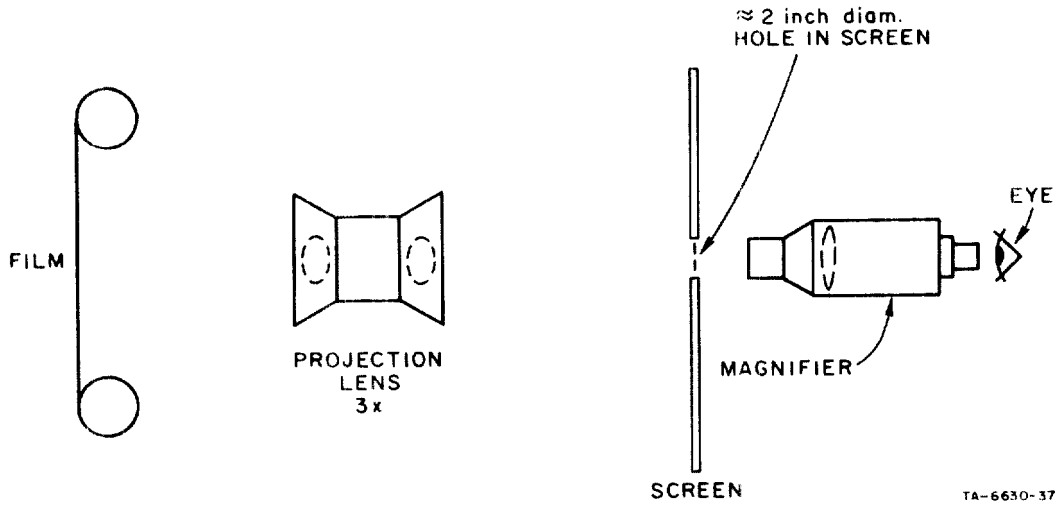

FIG. 23 REAR-SCREEN PROJECTOR WITH AUXILLIARY MAGNIFIER TO ACHIEVE HIGH MAGNIFICATIONS

The fundamental difference between auxiliary magnification and direct magnification of the image on the screen is the elimination of the screen and the addition of the eye, which contributes a three-diopter range of accommodation to the overall optical system (film to retina). In the direct screen magnification system, errors in precise focus of the film image on the screen result in a defocused image and a loss of resolution, for which the eye can in no way accommodate. A small error in focus results in a shift in the position of critical

focus for the screen image. With the screen position fixed, this shift results in the defocused screen image. On the other hand, without the screen the projected image remains sharply focused and a magnified examination is possible using the eye/magnifier combination. Small shifts in the position of the image can be kept in sharp focus on the retina either by moving the magnifier or by eye accommodation.

The required eye accommodation in diopters (D) to focus upon a pattern located a distance p in front of a magnifier when the eye is located at a distance f_1 behind the magnifier (see Fig. 24) is given by*

$$D = D_1\left(1 - \frac{p}{f_1}\right)^* \quad , \tag{3}$$

where D_1 is the eye accommodation required when p = 0 (object against the lens). Thus, D_1 is simply $1/f_1$, where f (magnifier focal length) is in meters.

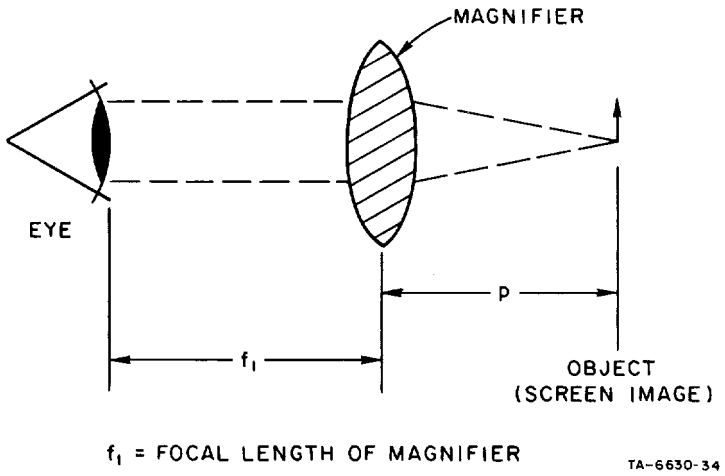

FIG. 24 MAGNIFIER LAYOUT USED IN COMPUTATION OF EYE ACCOMODATION/IMAGE MOVEMENT RELATIONSHIP

*Derived in Ref. 2.

This simple relationship can now be extended to relate the normal range of a three-diopter eye accommodation to the allowable film plane focus error as a function of the total film image magnification. The total magnification is the basic 3X screen magnification (m_0) times the magnifier magnification (m_1). The magnifier magnification is normally defined as

$$m_1 = 10/f_1 \tag{4}$$

when f_1 is in <u>inches</u>, or

$$m_1 = 0.25/f_1 \tag{5}$$

when f_1 is in <u>meters</u>.

The focus-detection masks are located in an equivalent plane of the screen image; therefore, the focus-error signals are measured with respect to this plane. (Section II-D-2 explains this point in detail.)

The ±0.001 inch peak-to-peak focus error shown in Fig. 1 with the film stationary represents a screen image displacement of m^2 times this value, or ±0.010 inch. Therefore, the total screen image displacement of 0.020 inch can be treated as the change in p in Eq. (3).

The following substitution will be made in Eq. (4). Let

$$D_1 = \frac{1}{f_1}$$

$$f_1 = \frac{0.25}{m} \quad \text{(from Eq. 5)}$$

$p = f_1 - \Delta$ (where Δ is the allowable change in p for a given allowable eye accommodation)

D = eye accommodation required in diopters.

Then from Eq. (3)

$$D = \frac{1}{f_1}\left[1 - \left(\frac{f_1 - \Delta}{f_1}\right)\right]$$

$$D = \frac{\Delta}{(f_1)^2}$$

$$D = \frac{\Delta(m_1)^2}{0.62} \quad .$$

Therefore,

$$\Delta = \frac{0.062\ D}{m_1^2} \quad . \qquad (6)$$

Δ can be equated to the screen image motion and m_1 is the magnifier magnification. The equation can be extended to include total film image magnification by substituting for Δ

$$\Delta = \delta(m_0)^2$$

where

δ = lens-to-film focus error,

and

m_0 = film-to-screen image magnification.

The resulting equation is

$$\delta = \frac{0.062\ D}{(m_0\ m_1)^2} \quad . \qquad (7)$$

Converting the units used from meters to inches results in

$$\delta_{inches} = \frac{2.5\ D}{(m_0\ m_1)^2} \quad . \qquad (8)$$

The total magnification of the film image is $m_0 m_1$. A parametric plot of Eq. (8) for two values of allowable eye accommodation is shown in Fig. 25 with m_0, the fixed screen magnification, equal to 3, and for m_1, the magnifier, a range from 3X to 40X. The total image magnification thus covers a range from 0 to 120.

The horizontal line on the graph of Fig. 22 at a δ of 0.002 indicates the potential focus accuracy of the present demonstration unit and shows that if the normal 3 diopters of eye accommodation were allowed,

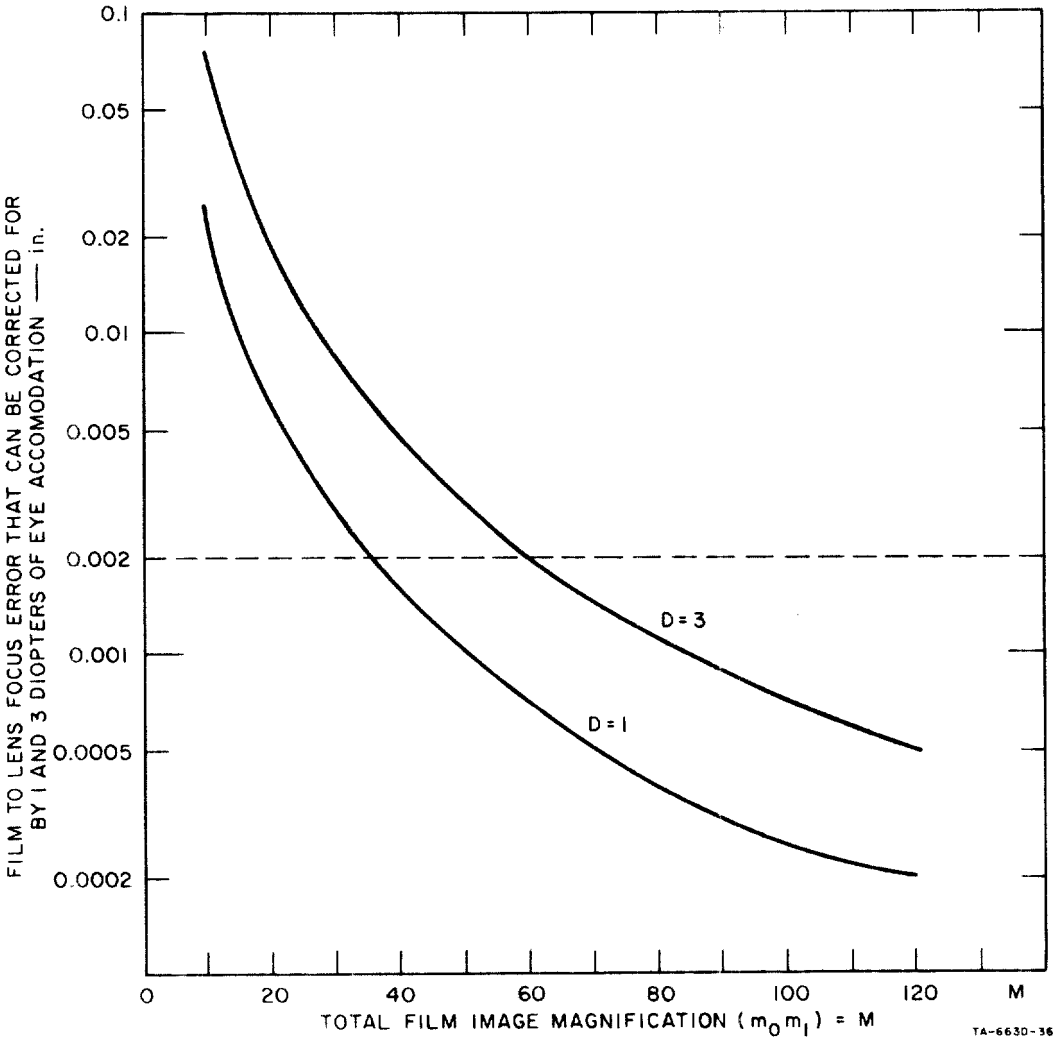

FIG. 25 ALLOWABLE FOCUS ERROR AS A FUNCTION OF MAGNIFICATION FOR ONE AND THREE DIOPTERS OF EYE ACCOMODATION

an overall magnification of 60X could be achieved without focusing the magnifier or loss of image resolution.

The second major consideration to be evaluated and compared for the two methods of achieving high magnifications is the area of the film that would be visible at one time in the field of view of the magnifier as a function of the magnification. The 3X screen image presents an entire 9 X 9 frame on a 27 X 27 inch screen for full viewing of the entire frame. When the magnification of the screen image is increased by shortening the projector lens focal length, the 27 X 27 inch screen area will provide a picture of a portion of the negative whose area is related to the area of the total negative by the equation

$$\frac{\text{Area of the negative shown on screen}}{\text{Area of the total negative}} = \left(\frac{m_0}{m_0\, m_2}\right)^2 \qquad (9)$$

where

$m_0 = 3\times$

and

m_2 = the additional magnification factor (numerically equal to the m_1 of the auxiliary magnifier used in the alternate method of obtaining high magnifications just described).

To determine the relative picture area seen through the magnifier as a function of m_1 requires:

(1) Determination of the area of a realistic field of view for a magnifier at a given m_1, and

(2) The reasonable assumption that as m_1 changes, the area of the field of view of the magnifier will decrease as $1/m_1^2$.

A conservative estimate can be made by taking the field of view presently covered by a wide-field, 1.5-inch-focal-length eyepiece available in the laboratory. This eyepiece used as a magnifier has a $m_1 = 10/1.5 = 6.7$ and covers a 2-inch diameter field of view.

In the preceding example with $m_2 = 6.7$, the relative area of the negative covered is

$$\frac{1}{(6.7)^2} = 0.0225 \quad .$$

For the magnifier described above, the relative area covered is

$$\frac{\pi(1)^2}{27 \times 27} = 0.0037 \quad .$$

The ratio of these relative <u>areas</u> is

$$\frac{0.0225}{0.0037} = 6.1 \quad .$$

The <u>linear</u> reduction in the field of view is $\sqrt{6.1} \cong 2.5$. Thus, the use of the auxiliary magnifier results in a surprisingly small reduction in the field of view at higher magnifications. In addition, this may be more than offset by the fact that a minimum area of 25 percent of the full negative remains in view on the 3× screen image for use in orientation.

A potential disadvantage associated with the use of the auxiliary magnifier is the change in viewing posture required when going from the 3× scanning mode to the higher magnifications. Basically, the change requires leaning forward 10 to 15 inches from the normal screen viewing position and looking into the magnifier.

An opinion of the significance of this in operational terms can only be inferred from very limited experimental viewing. It is possible that this system would offer operational advantages. Only with further experience using a system based on this approach could a more quantitative judgment be made as to relative advantages and disadvantages of using two viewing modes.

There are a number of significant advantages with this system.

(1) A change from the full frame 3X screen image to a given* higher power requires no change of any kind within the projector. Both magnifications are presented and in focus at all times. Thus, orientation of the high-magnification image can easily be made with respect to the large area low-power image that is presented on the screen. (The minimum frame area of 25 percent only occurs when the magnified area is in a frame corner. The X-Y positioning of the film carriage places the corner of the 3X picture at the center of the screen and, hence, only 25 percent of the frame is visible on the screen.)

(2) Maximum resolution is possible since there is no diffusing screen in the optical path and both the 3X projection lens and the magnifier are straightforward optical designs capable of excellent resolution.

(3) Image brightness at high magnification is excellent, without requiring excessive illumination power to maintain screen brightness at high magnification.

(4) All the required system components, including the automatic focus detection and the lens servo, can be engineered and constructed in a straightforward manner. The relative simplicity of all the component subsystems would provide a much lower cost projector with a performance capability for rapidly scanning aerial film at low magnification, yet providing for quick high-resolution examination of interesting film areas.

*Readily interchangeable magnifiers of several powers or a zoom magnifier can easily cover the desired range of higher magnification.

V CONCLUSIONS AND RECOMMENDATIONS

A. Conclusions

1. A demonstration model of a rear-screen projector with automatic focus detection and control has been successfully built and tested. The basic problems associated with the system integration of the subsystems have been solved. The desired sensitivity of focus detection and control have been achieved, but not the required accuracy.

2. The major remaining source of error in the focus-detection subsystem is a rear-surface film reflection. Straightforward techniques to modify the focus-detection subsystem suggested in the text, when implemented, would reduce the error to a value equal to ±1/4 the film thickness. An extension of the outlined modifications should permit a further reduction in the error by at least a factor of three to five.

3. The application of the focus-detection technique to an advanced state of the art rear-screen projector employing high-screen magnification and film transport mechanisms that clamp the film between glass platens would be of marginal value. The predicted focus-detection accuracy thus achieved would not provide a significant increase in performance for the added complexity of an already expensive projector.

4. The application of automatic focus detection to a fixed 3× screen magnification projector with a film transport using no platens is both feasible and potentially attractive. A simple, low-cost rear-screen projector could make use of an auxiliary magnifier for high-magnification, high-resolution examination of a small central area of the screen image.

B. Recommendations

1. It is recommended that consideration be given to establishing a modest program to determine and evaluate both the potential usefulness and the specifications for a simple low-cost rear-screen projector. The basic concept, described in Sec. IV-B-2, would employ a fixed 3×

screen magnification combined with auxiliary magnification of a central image area where the screen has been removed. This will permit a bright, high-resolution magnified examination to be made of any selected portion of the image.

2. The application of direct viewing magnifiers in a clear center area of the image screen to the next generation of rear-screen projectors should also be evaluated. Because of the magnified screen images available, the auxiliary magnifiers could be of low power (3X to 6X) and cover a wide field. The elimination of the screen and the increased brightness of the image would make possible a critical overall high magnification examination of the image. By achieving the highest magnification as the product of the auxiliary magnifier and the screen image, the maximum screen magnification could be reduced.

Appendix A

LENS SERVO SUBSYSTEM

1. DESIGN REQUIREMENTS

As the film drive moves the film through the projector for scanning, the film deviates from the nominal film plane of the projector, thus resulting in a loss of sharp focus on the screen. To restore and maintain sharp focus despite motion of the film plane, a servo system was designed to move the projection lens so as to maintain the entire optical system in focus.

For purposes of the initial servo system design, the following input and performance specifications were stipulated:

(1) The film deviates from its nominal position by ± 1/16 inch, with significant flutter frequencies up to 5 c/s.*

(2) The lens servo must exhibit a static accuracy sufficient to position the lens within 0.001 inch of the lens/film separation for sharpest focus.

(3) The lens servo must compensate for at least 50 percent of the maximum film motion (± 1/16 inch) at 5 c/s (i.e., the system 3-DB bandwidth shall be at least 5 c/s).

2. SYSTEM DESIGN

The functional design of the lens servo system to satisfy these requirements is illustrated in Fig. A-1. It is basically a null-seeking

*Strictly speaking, the lens motion is not an exact duplicate of the film motion; however, for design purposes, this is an excellent approximation.

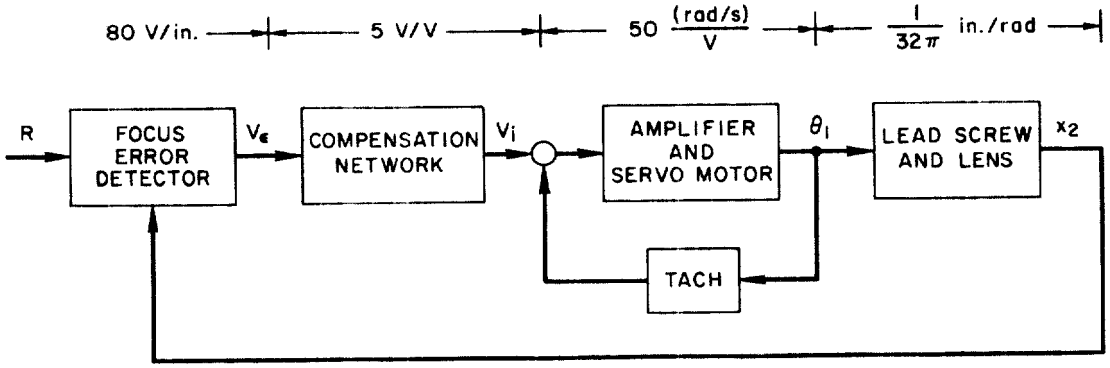

R = FILM POSITION
x_2 = LENS POSITION
V_ϵ = LENS POSITION ERROR SIGNAL - 80 V/in. OF LENS DISPLACEMENT FROM POSITION OF SHARPEST FOCUS
V_i = SERVO SYSTEM INPUT VOLTAGE
θ_l = SERVO MOTOR SHAFT POSITION (radians)

TA-6630-26

FIG. A-1 SERVO SYSTEM BLOCK DIAGRAM

Type I position servo with an inner tachometer feedback loop employed to improve the performance characteristics of the servo motor, and ensure adequate overall system stability.

The focus detection subsystem, whose design and operation have been described in Sec. II-D, provides a servo system input signal whose magnitude and polarity at each instant are proportional to the lens position relative to its position of sharpest focus. The proportionality factor of the focus detector as currently implemented is 80 V/inch of lens position error.

The focus-detector output signal is processes by the compensation network to provide adequate dc gain and appropriate shaping of the frequency characteristic. This network is realized using operational amplifiers so as to render its properties independent of the parameter values of the individual active elements. Two compensation networks were tested during the prototype development. The initial design employed simply gain compensation and produced the open-loop response characteristic shown on curve A of Fig. A-2. An instability due to an unexpected structural resonance required modification of the frequency

response by the inclusion of a lag-lead filter, with the resulting open-loop characteristic shown on curve B of Fig. A-2. The dc gain of the compensation network was experimentally set at 5 V/V.

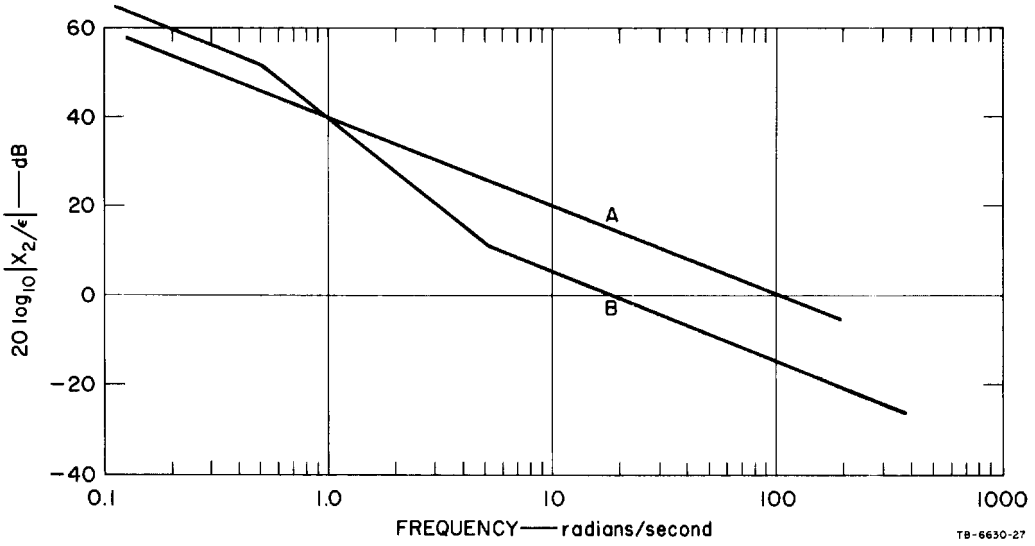

FIG. A-2 OPEN-LOOP FREQUENCY CHARACTERISTICS

A 400-c/s two-phase servo motor with integral tachometer was chosen as the output drive element to obtain a low motor inertia and a reasonably linear torque-speed characteristic. Tachometer feedback around the servo motor and its drive amplifiers tends to reduce the effects of the inherent electrical and dynamic lags and makes the motor behave more like an ideal integrator. Four-hundred c/s power for the motor is obtained via two conventional audio power amplifiers; one driven directly from the reference oscillator and supplying the motor reference phase, and the other driven by the chopped error signal and supplying the motor control phase.* The overall motor-tachometer-loop exhibits a dc gain of 50 radians/s/V.

*This is shown in detail in the schematic diagram, Fig. A-3.

The rotational output of the servo motor is converted to linear translation of the lens by means of a ball bearing lead screw driving a ball bearing slide. This combination provides a minimum of friction while at the same time eliminating backlash. The lead screw thread is 16 turns/inch, thus yielding a conversion factor of $1/32\pi$ inch/radian.

The detailed dynamics of the servo motor-tachometer loop and the overall position loop are shown (in Laplace transform notation) in Figs. A-4(a) and (b).

3. SERVO SYSTEM TESTS

The completed servo system was tested and its properties determined by subjecting the system to controlled inputs. Motion of the film was simulated by mounting a piece of film on a linear actuator to permit the generation of accurately known film motions.

In initial testing, a square wave displacement was imparted to the film and the servo system parameters adjusted to obtain a 20 percent first overshoot, which corresponds to a damping factor of approximately 0.5 for a nominal second-order response. With the system thus adjusted its sinusoidal frequency response was measured for a film displacement of ± 1/16 inch. The resulting response characteristic is shown in Fig. A-5. The 3-dB bandwidth is measured to be 3.6 c/s, and the velocity constant is approximately 100.

4. OPERATIONAL TESTING

At the completion of the above tests, the linear actuator was replaced by the film transport for the 9-inch aircraft film. This transport is designed such that there is a 9 × 9-inch unsupported film area. A mechanical resonance in the projector structure caused a coupling of energy from the lens servo to this unsupported film area. This caused the film-servo system to oscillate at 40 c/s with the system gains set as in the previous tests. To correct this situation, the system open-loop frequency characteristic was modified by adding a lag-lead filter to the compensation network, as shown in Fig. A-2.

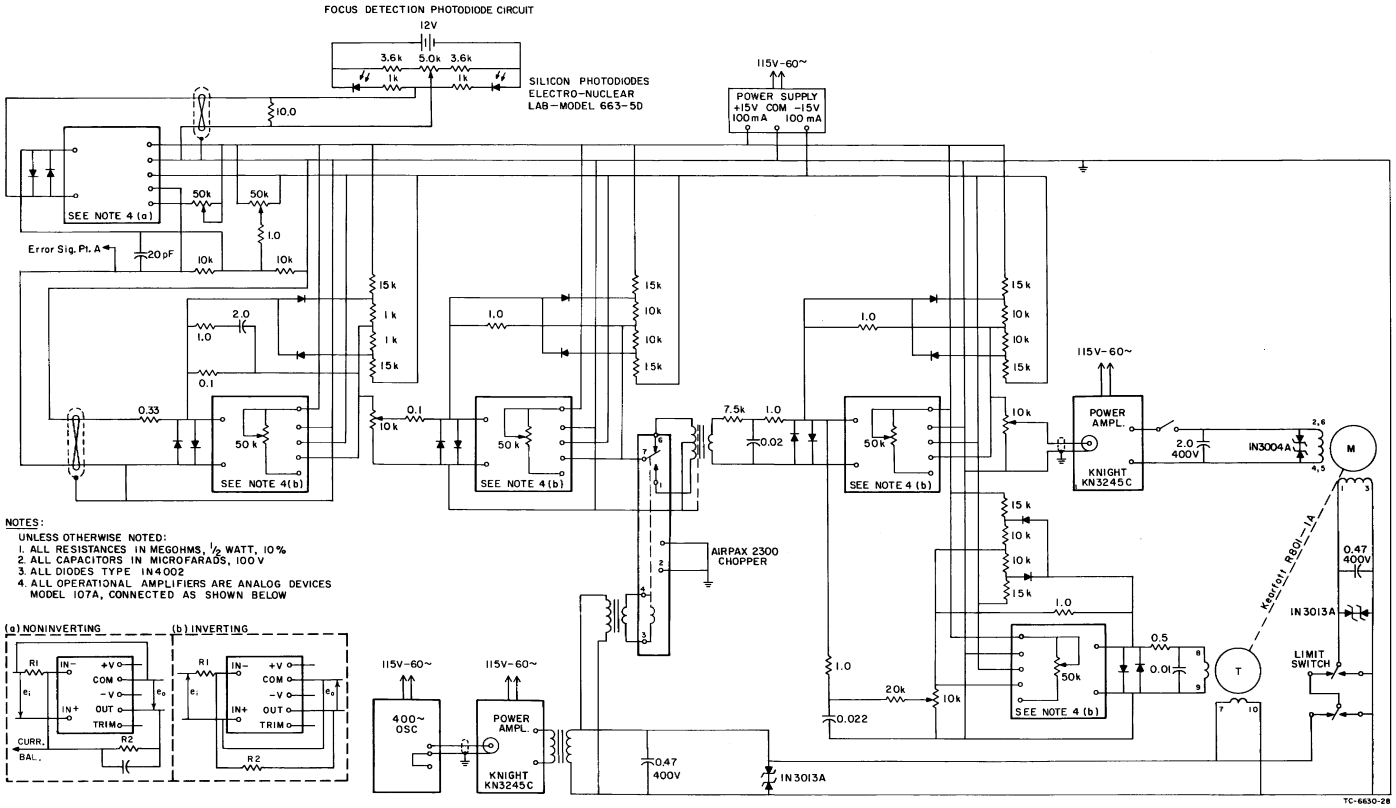

FIG. A-3 SCHEMATIC DIAGRAM OF SERVO SYSTEM

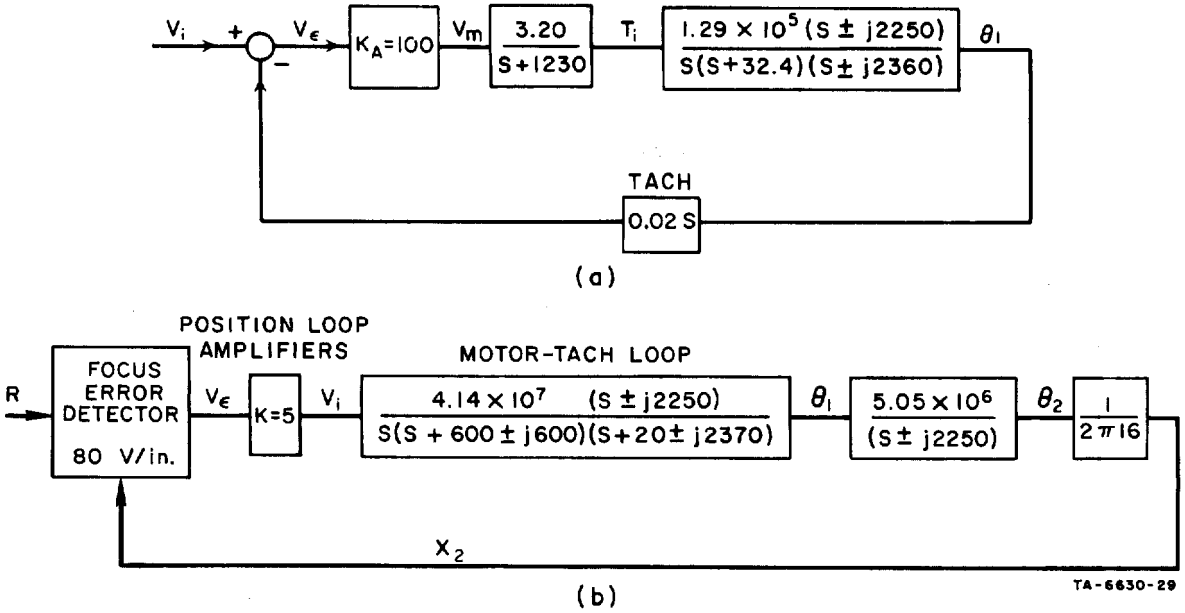

FIG. A-4 SERVO SYSTEM DYNAMICS
(a) Servo motor/tachometer loop dynamics
(b) Position loop dynamics

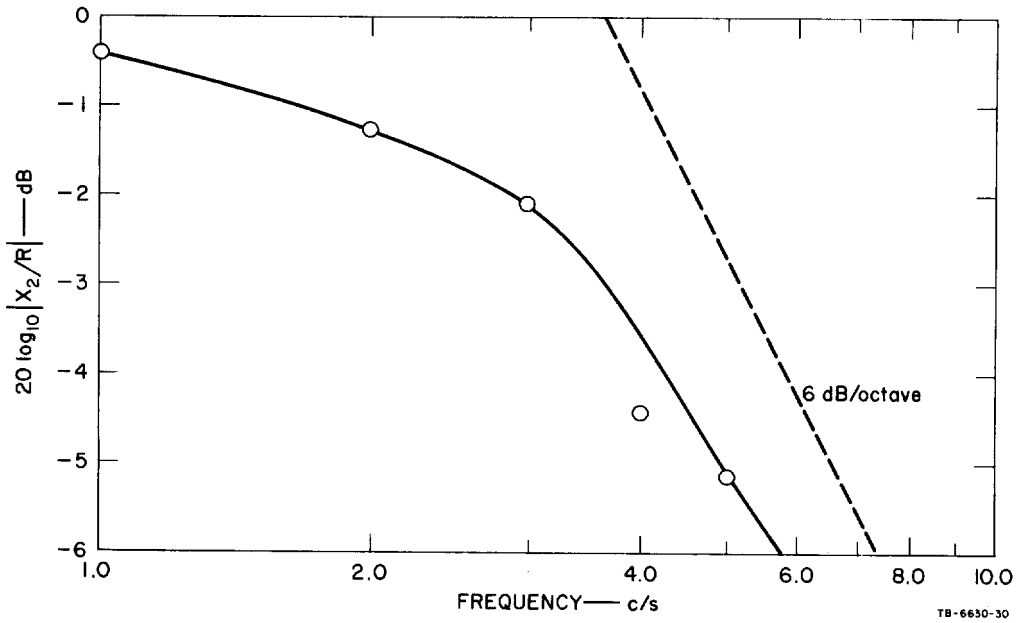

FIG. A-5 CLOSED-LOOP SINUSOIDAL FREQUENCY RESPONSE

In its final configuration, the servo system maintained focus error for stationary film at less than 0.0002 inch. Step changes in the film plane position gave rise to focus error signals that demonstrate a servo system damped natural frequency of approximately 2 c/s and a damping factor of approximately 0.5.

Appendix B*

A RECIPROCAL OPTICAL SYSTEM FOR MEASURING THE STATE OF FOCUS OF REFLECTED IMAGES

1. INTRODUCTION

The material presented in this appendix is a continuation and refinement of the basic focused detection theory developed during the preceding project and presented in the final report for that project, "Automatic Focusing Techniques."[1]

This extended treatment was developed independently of the present project effort for submission as a technical paper to an optical society journal. Because of its relevance to this project and to future application of automatic focusing techniques to rear-screen projectors, this version of the paper is appended to this report.

STAT In an earlier work, [redacted] (1964) described a passive ranging device based on the use of a sandwich-type nonlinear photocell. In that scheme, the full image is made to fall on the face of the photocell [as shown in Fig. B-1(a) for the case of a point source], and the output is in terms of the conductance measured between the two plates of the cell (one plate of which is transparent). As the photocell is moved along the optic axis, the total light captured by the photocell is invariant, although the distribution of light is continually changing. If the photocell is linear, in the sense that $g(x,y) = K \cdot I(x,y)$, where g and I are the point conductivity and point light intensity, respectively (and K is a constant), then the total conductance of the cell, $G = \iint g(x,y)\, dx\, dy$, is proportional only to the total light falling on the cell--i.e., $G = K\iint I(x,y)\, dx\, dy$--and is independent of the distribution of light. If the local conductance

STAT [redacted]

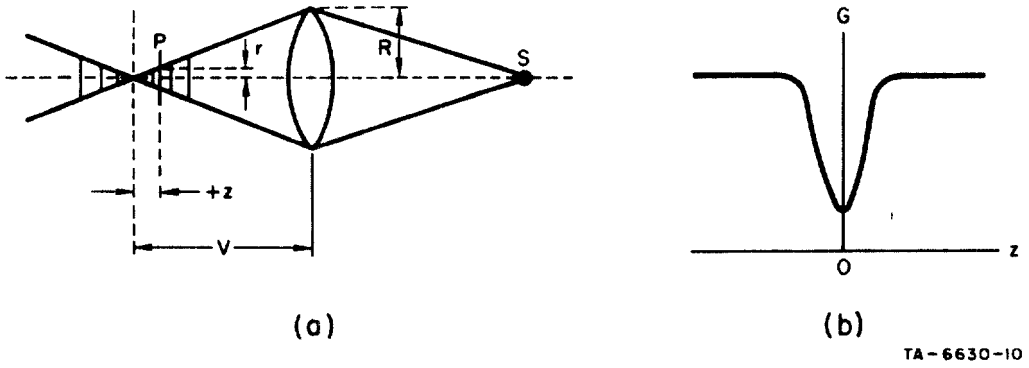

FIG. B-1 DEFOCUSED IMAGE FALLING ON PHOTOCELL SURFACE P
(a) Geometry
(b) Photocell conduction as a function of axial position

is a nonlinear function of light intensity, however (e.g., a logarithmic dependence), then the total conductance G is sensitive to the light distribution, as suggested in Fig. B-1(b), even though the total light falling on the cell is constant.

Given the characteristic of Fig. B-1(b), the state of focus can be detected simply by vibrating the cell along the optic axis. Because of the even symmetry of the characteristic, the output signal will have one phase or the other depending on the direction of defocus--i.e., whether $z > 0$ or $z < 0$, where z is the distance that the photocell is from the plane of best focus--and will be folded-over when the image is in-focus ($z = 0$). In Fig. B-2 it is shown that this same result is obtained from a general image as well as from just a single point source.[4] In Fig. B-2(a) are a set of images falling on the photocell as a person approaches the lens, with a parking lot in the background, and in Fig. B-2(b) are the corresponding output signals from the photocell. In this case the photocell is vibrating about a fixed image plane corresponding to an object distance of 6 ft. Note that when the front surface of the subject is at 6 ft there is a strong double-frequency (i.e., folded over) signal, as predicted; at 5 ft and 7 ft the signal is at the fundamental frequency, but with opposite phases.

Automatic-focus systems have been attempted on the basis of this type of scheme ([redacted]), though with limited success; one

STAT

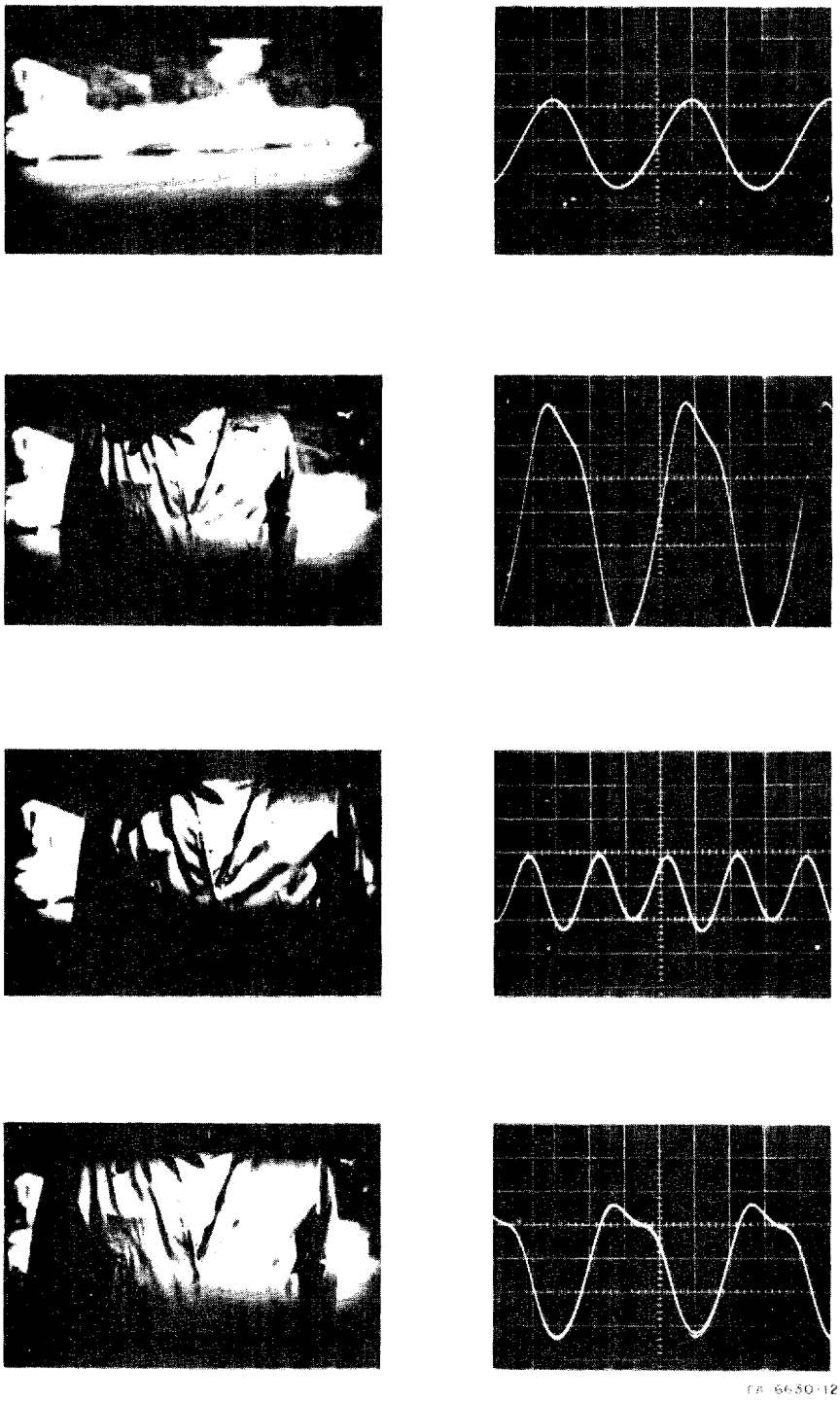

FIG. B-2 PHOTOCELL SIGNAL FOR DIFFERENT DISTANCES BETWEEN OPTICAL SYSTEM AND APPROACHING MAN

difficulty is that with wide-area images, as in Fig. B-2 (i.e., images larger than the photocell), vignetting can cause confusion because of changes in total light falling on the photocell. But in any case, schemes of this type depend on the image containing some minimum amount of contrast pattern, and would therefore not be useful in cases where we wished to monitor the distance, say, to a uniformly illuminated wall. If the wall, or surface, were reflective, however, we could attempt to measure its distance by projecting an image onto it and determining the state of focus of the reflected image.

2. A RECIPROCAL IMAGING SYSTEM

Essentially, what we need to do to determine the state of focus is to compare the reflected image with the original pattern. One way to do this is to arrange for the reflected image to fall directly onto the original pattern. Suppose, for example, that the input pattern is formed by illuminating a circular cutout W, in an opaque sheet O, as in Fig. B-3. The real image of the object, formed by the lens, is reflected by the mirror M. The reflected image will act as a new source,

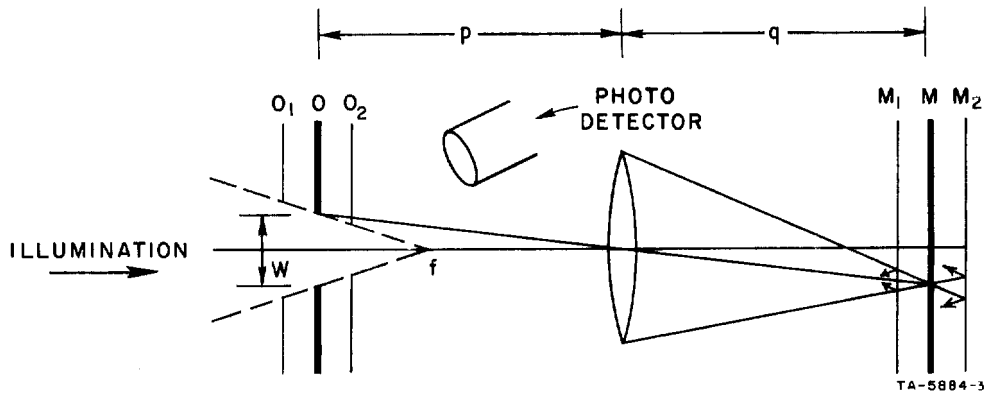

FIG. B-3 DETECTION OF INTERCEPTED LIGHT IN OBJECT PLANE

which in turn is imaged by the lens. If the mirror were located in the in-focus image plane, then, ideally, the new image (by optical reciprocity) would fall exactly on the original object, and all of the light

reflected through the lens would pass back through the aperture. (This result holds independently of the shape of the cutout.) If the mirror is shifted along the optical axis (e.g., to position M_1 or M_2), the distance between the first real image (considered now as a source) and the lens changes, causing a corresponding axial shift of the position of the second image (to position O_1 and O_2, respectively). Viewed from the original object plane, the second image now appears defocused, and in this case a certain amount of the reflected light is intercepted by the opaque screen. Nominally, the more out of focus, the larger the magnitude of intercepted light. Thus, a plot of intercepted light would have the same basic form as the conductance plot of Fig. B-1(b). This conclusion holds even if the input pattern is moved off axis, since every point of the input pattern images back on itself. This is one of the principal features of the reciprocal optical system, i.e., it is a self-aligning system.

For the experimental curves shown later, the surface of the opaque sheet that faces the lens was painted white, to serve as a diffuse reflector for intercepted light, and a portion of this diffused light is received by the photodetector, as suggested in Fig. B-3. (More accurate measurement of the intercepted light could be obtained, if necessary, if the entire surface of the opaque sheet were, for example, coated with a photoconductor.) For purposes of our analysis here, we will assume that the photodetector does in fact collect all of the light intercepted by the opaque sheet.

What we are interested in finally is using the intercepted light to monitor movements of the mirror along the optic axis. Our main job of analysis therefore is to determine how the magnitude of intercepted light varies as a function of mirror position. For design of a focus-detection (or automatic-focus) system, we would also have to know how this function changes with system parameters; in particular, the magnification ratio, p/q, and the size of the object. We would also like to know how sensitive the function is to lateral displacement of the object, and to angular changes of the mirror with respect to the optical axis.

Note that with a diffuse reflector--e.g., a piece of white paper--in place of the mirror, the first image is itself defocused whenever the reflector is outside of the image plane. The second image formed by the lens is then a focused version of the first defocused image. Viewed from the original object plane we now have a defocused version of the second image, and this is then doubly defocused. In this appendix we treat only the case of specular reflection, i.e., the single defocus case. For double defocus the results are actually very similar, although the analysis is somewhat more complex. (For some discussion of the double-defocus case, [redacted] STAT

In the following sections we derive analytic expressions for both the total light returned through the lens and for the light intercepted by the aperture mask, as a function of mirror position (Δq_M), with magnification (p/q) and the ratio of diameters of aperture and lens (W/D) as major parameters. We will see that the experimental data are, in fact, accurately predicted by the analysis.

3. ANALYSIS OF THE OPTICAL SYSTEM

What is required in the analysis is a basic understanding of the form of the reflection for any point P of the input pattern. In Fig. B-4, input point P is imaged as point Q. All of the light reaching Q, in incident bundle I, is reflected about the normal N drawn to the mirror at Q. A first important effect to note is that of all the light in the reflected bundle R, only a portion R′ is actually reimaged at point P. The remainder misses the lens entirely and is lost. The percentage of light lost in this fashion increases with the angular displacement θ of the input point.

If the mirror moves axially by an amount Δq_M (Fig. B-5) then the image of the source is formed at Q′, a distance $\Delta q = 2\ \Delta q_M$ in front of the original image plane, and point Q′ is in turn reimaged as P′, displaced an amount Δp from the original input plane. Point Q′ is displaced from the optical axis by exactly the same amount as point Q, but since Q′ is closer to the lens, the angular displacement θ' of the image

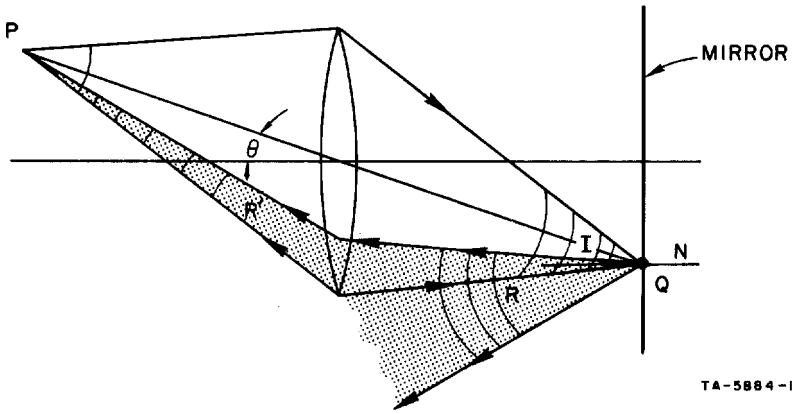

FIG. B-4 INCIDENT CONE I AND REFLECTED CONE R FROM MIRROR

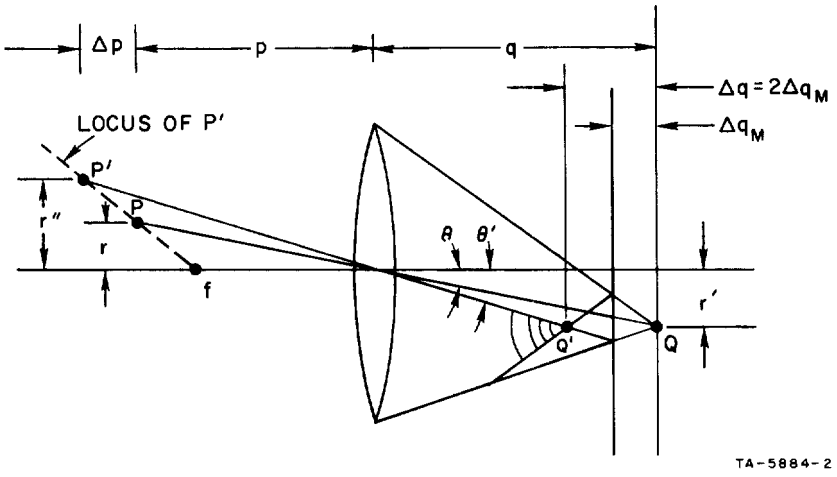

FIG. B-5 CHANGE IN MAGNIFICATION WITH MIRROR MOVEMENT Δq_M

point is larger than the angular displacement θ of the original object point.

To find the relation between Δp and Δq we simply subtract the equations for the first and second imaging, namely

$$\frac{1}{f} = \frac{1}{p} + \frac{1}{q}$$

$$\frac{1}{f} = \frac{1}{p + \Delta p} + \frac{1}{q + \Delta q} \quad , \tag{B-1}$$

from which we derive the expression

$$\frac{\Delta p}{p} = \frac{-\, p/q}{\frac{q}{\Delta q} + \frac{p}{f}} \quad , \tag{B-2a}$$

or, equivalently,

$$\frac{\Delta q}{q} = \frac{-\, q/p}{\frac{p}{\Delta p} + \frac{q}{f}} \quad . \tag{B-2b}$$

Note that p and q are each defined as positive in the direction away from the lens, so that a $(+\Delta p)$ corresponds to a $(-\Delta q)$. If P is located a distance r from the optic axis, then the first image point Q is displaced from the axis by a distance

$$r' = (q/p)r \quad , \tag{B-3}$$

and P' is displaced from the axis by an amount

$$r'' = \left(\frac{p + \Delta p}{q + \Delta q}\right) r' = r \left(1 + \frac{\Delta p}{p - f}\right) \quad . \tag{B-4}$$

From Eq. (B-4) we see that the reimaged point P' falls along a line drawn through the source point P and the focal point of the lens, as shown by the dashed line in Fig. B-5. Or, in terms of Δq, substituting Eq. (B-2),

$$r'' = r \left(\frac{1}{1 + \frac{\Delta q}{q}\frac{p}{f}}\right) \quad . \tag{B-5}$$

Equations (B-2) and (B-5) will be used to determine the returned image size and position as a function of mirror position Δq_M. This will be important in computing the intercepted light function L_I.

a. Total Returned Light

We first determine the total amount of light returned through the lens as a function of mirror position. At any given mirror position, the amount of light returned from a point within the source depends on the distance r of that point from the axis. For example, if $\Delta q_M = 0$ (i.e., the mirror is at the focal position), we have the condition depicted in Fig. B-6; the circular cone of light coming to focus

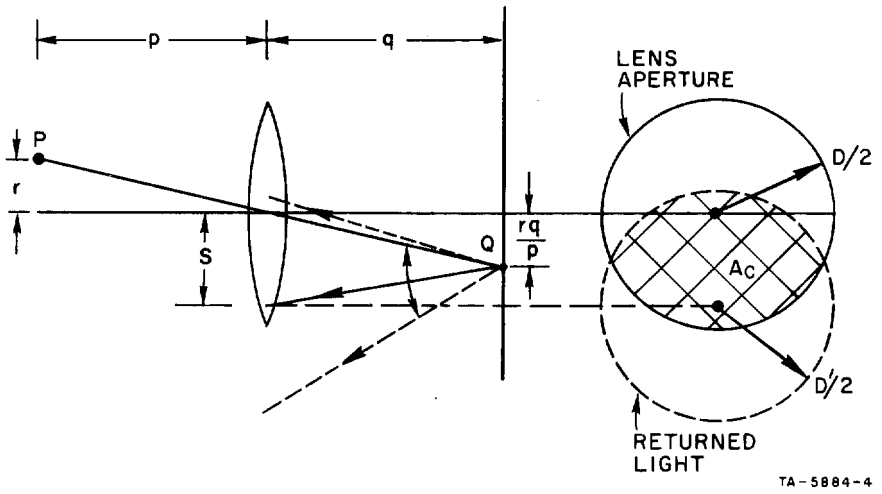

FIG. B-6 RETURNED-LIGHT DISK IN LENS PLANE

at image point Q is reflected by the mirror, and intersects the lens plane as a disk having exactly the same diameter as the lens but displaced from the optical axis by a distance

$$S = 2r' = 2r\,\frac{q}{p} \quad . \tag{B-6}$$

The light that passes back through the lens is represented by the common cross-hatched area A_c. Thus, the returned light has a maximum value for $r = 0$ (in which case the two circles in the lens plane are coincident), and decreases monotonically with r, becoming zero for $S = D$, where D is the lens diameter. This latter condition occurs for a value of r equal to

$$r_c = \frac{D}{2} m \quad , \tag{B-7}$$

where $m = p/q$ is the magnification ratio of the optical system.

As the mirror is moved along the optical axis, the diameter of the reflected light disk in the lens plane changes according to

$$D' = D \left(1 + 2 \frac{\Delta q_M}{q}\right) \quad . \tag{B-8}$$

Thus $D' < D$ for negative Δq_M (movement toward the lens) and $D' > D$ for positive Δq_M (movement away from the lens). The returned light is again represented by the common area (in the lens plane) of the returned light cone and the lens circle, as shown in Fig. B-7, where the separation S is now generalized to the form

$$S = \frac{2r}{m} \left(1 + \frac{\Delta q_M}{q}\right) \quad . \tag{B-9}$$

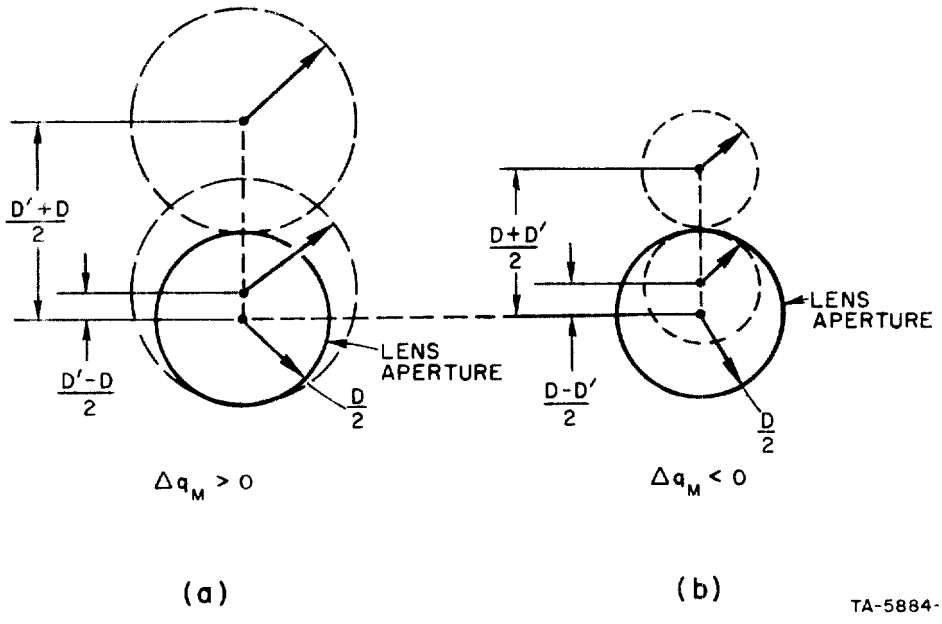

FIG. B-7 RELATIONSHIP OF LIGHT DISK AND LENS DISK WITH MIRROR OUTSIDE IMAGE PLANE

We now consider the total light return for an input disk object of diameter W. This is determined by integration of the light returned from each point within the input disk. Consider an infinitesimal area dA of the input disk. Light from this point is collected by the lens to form the imaging cone I of Fig. B-4, which is reflected by the mirror to produce the reimaging cones R and R′, which in turn forms an image dA′′ at point P′, Fig. B-5. For a point on the center of the input disk, and for the mirror in the focal position, all of the light in the cone R is collected by the lens; thus, the light flux contained in cone R is equal to that contained in R′ and I. If the luminous intensity at the center of the returned image is denoted by I_o, then the light flux contained in cone R′ (and therefore R and I) is $I_o dA'' = I_o dA$ (since $dA'' = dA$ when $\Delta q_M = 0$). It is important to note that (except for second-order effects for points far from the axis) the light flux contained in cones I and R is independent of the location of P in the object plane, and the position of the mirror along the axis, and is therefore equal to $I_o dA$ for all values of r and Δq_M. Thus, the illuminance in the lens plane produced by reimaging cone R is given by

$$E_L = \frac{I_o dA}{\pi D'^2/4} \quad , \tag{B-10}$$

independent of r.

The light flux returned by the lens for any point in the source is then

$$L_i = A_c(D,D') \cdot \frac{I_o dA}{\pi D'^2/4} \tag{B-11}$$

where $A_c(D,D')$ is the common area between D and D′. For a uniformly illuminated circular disk, we can express the total returned light L_T as

$$L_T = I_o \int_0^{W/2} \frac{A_c(D,D')}{\pi D'^2/4} \cdot 2\pi r dr \quad . \tag{B-12}$$

In Eq. (B-12), $A_c(D,D')$ is a function of D, D′, and S; the latter two quantities are found from Eqs. (B-8) and (B-9). (A general derivation

of the common area A_c is given in Annex 1.) It should be noted that for $S < |(D - D')/2|$ the smaller disk is completely contained within the larger disk, and the common area is simply equal to the area of the smaller disk; also, that for a disk source, the largest values of S are obtained from input points at the edge of the disk, i.e., at $r = W/2$ in Eq. (B-9). We can find values of Δq_M such that even for $r = W/2$, S never exceeds $|(D - D')/2|$; such values of Δq_M are found by setting $r = W/2$ in Eq. (B-9) and requiring that

$$\frac{D - D'}{2} \geq \frac{W}{m}\left(1 + \frac{\Delta q_M}{q}\right) \qquad \text{for } \Delta q_M < 0 \text{ , where } D > D' \text{ ,}$$

and

$$\frac{D' - D}{2} \geq \frac{W}{m}\left(1 + \frac{\Delta q_M}{q}\right) \qquad \text{for } \Delta q_M > 0 \text{ , where } D' > D \text{ .}$$

These conditions, in conjunction with Eq. (B-8), lead directly to the results

$$\frac{\Delta q_M}{q} \leq \frac{-\alpha}{1 + \alpha} \quad , \quad \text{for } \Delta q_M < 0 \quad ; \qquad \text{(B-13a)}$$

$$\frac{\Delta q_M}{q} > \frac{\alpha}{1 - \alpha} \quad , \quad \text{for } \Delta q_M > 0 \quad ; \qquad \text{(B-13b)}$$

where

$$\alpha = \frac{W}{D} \cdot \frac{q}{p} \quad . \qquad \text{(B-14)}$$

For the condition given by Eq. (B-13a), $A_c(D,D') = \pi D'^2/4$ for all input points, and Eq. (B-12) simply becomes

$$L_T = I_o \int_0^{W/2} 2\pi r dr = I_o \, \pi \, W^2/4 \quad , \quad \text{for } \frac{\Delta q_M}{q} \leq \frac{-\alpha}{1 + \alpha} \quad ; \quad \text{(B-15)}$$

which is independent of Δq_M. For the condition of Eq. (B-13b) $A_c(D,D') = \pi D^2/4$ for all input points, and Eq. (B-12) becomes

$$L_T = I_o \int_0^{W/2} (D/D')^2 \, 2\pi r dr = (I_o \, \pi \, W^2/4) \cdot (D/D')^2 \quad , \qquad \text{(B-16)}$$

or, using Eq. (B-8),

$$L_T = \frac{I_o \, \pi \, W^2/4}{\left(1 + \frac{2\Delta q_M}{q}\right)^2} \quad , \quad \text{for} \quad \frac{\Delta q_M}{q} \geq \frac{\alpha}{1 - \alpha} \quad . \qquad \text{(B-17)}$$

The transition points given by Eq. (B-13) are significant in that they define the effective range for focus detection. For later reference these points are labeled as

$$\frac{\Delta q_{Mb}^-}{q} = \frac{-\alpha}{1 + \alpha} \qquad \text{(B-18)}$$

and

$$\frac{\Delta q_{Mb}^+}{q} = \frac{\alpha}{1 - \alpha} \quad . \qquad \text{(B-19)}$$

We see that for $\Delta q_M \leq \Delta q_{Mb}^-$, the total light returned has a constant value; for $\Delta q_M \geq \Delta q_{Mb}^+$ the total light returned varies inversely as the square of Δq_M. The range $\Delta q_{Mb}^- < \Delta q_M < \Delta q_{Mb}^+$ represents the transition between the two functions, and, as we will see, also defines the region where the light intercepted by the mask (Fig. B-3) differs markedly from the total returned light.

b. Intercepted Light

In the last section we determined the functional relation between the total light returned through the lens and the mirror position. We are primarily interested, however, in the magnitude of intercepted light (i.e., light that does not fall directly back onto the source object) as a function of Δq_M. We know that this function ideally is zero at $\Delta q_M = 0$, rising on either side of $\Delta q_M = 0$, eventually approaching the total light return as $|\Delta q_M|$ becomes large.

To determine the intercepted light L_I, consider again a point P on the disk object, located a distance r from the optic axis (see Fig. B-8). As we have seen, if the mirror moves by an amount Δq_M, then the reflected light is contained in a disk of diameter D' in the lens plane, whose center is displaced a distance S from the axis [see Eqs. (B-8) and (B-9)]. If $S > |(D - D')/2|$, then part of the D' disk is lost outside of the lens. This truncated cone in turn images at point P', a distance r'' from the axis, which as we saw in connection with Fig. B-5 lies along a line drawn through the point P and the focal point f. As this truncated cone passes the object plane (the p-plane), some of the light is intercepted beyond the edge of the original disk. It is this intercepted component of returned light that is of interest.*

The circles D and D' in the lens plane subtend, or generate, the circles W' and W'' in the object plane, and the separation S between D and D' in the lens plane subtends a distance S'' in the object plane. All object-plane dimensions are obtained directly from the lens-plane dimensions by the geometric ratio $\Delta p/(p + \Delta p)$; therefore,

$$W' = \frac{\Delta p}{p + \Delta p} D$$

$$W'' = \frac{\Delta p}{p + \Delta p} D' \qquad \text{(B-20)}$$

$$S'' = \frac{\Delta p}{p + \Delta p} S \quad .$$

The separation S', between the center of W (the input disk) and W' is found from Fig. B-8

$$S' = r'' \frac{p}{p + \Delta p} \quad . \qquad \text{(B-21)}$$

*Note that if the mirror is closer to the lens than 0.5 q, then the first image Q' lies on the p-side of the lens and the geometry of Fig. B-8 no longer applies, and the equations which follow are not valid. Since $\Delta q_M < - 0.5\ q$ is well outside of the range of interest, points beyond this extreme are not considered, and all of the following analysis should be interpreted as applying only to values of $\Delta q_M \geq - 0.5\ q$.

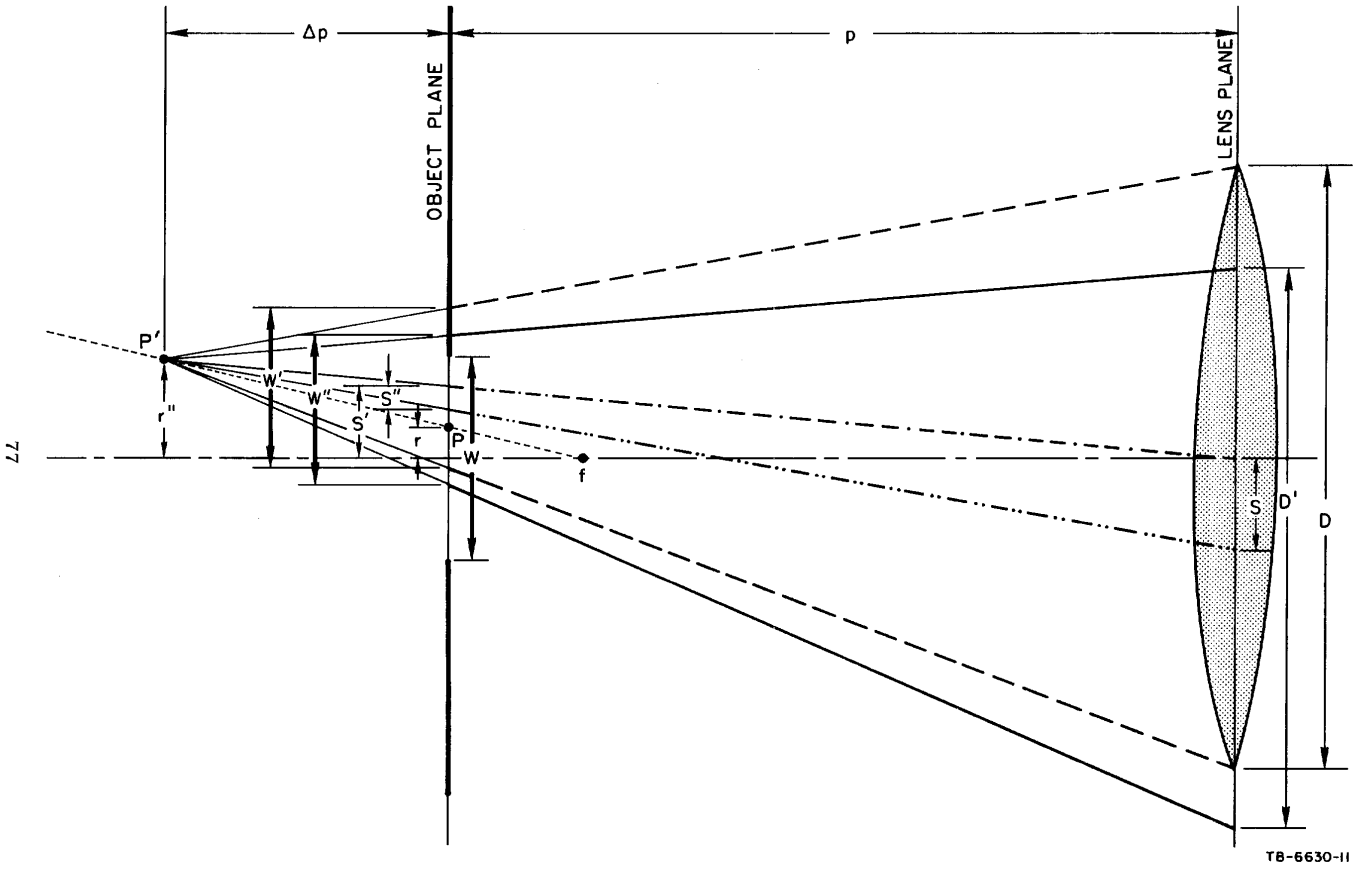

FIG. B-8 GEOMETRICAL RELATIONS FOR THE RETURNED IMAGE

These equations are written in terms of known parameters through the use of Eqs. (B-2), (B-5), (B-8), (B-9) for Δp, r'', D', S, giving

$$W' = \frac{W}{\alpha} \cdot \frac{2\Delta q_M/q}{1 + 2\Delta q_M/q} \tag{B-22}$$

$$W'' = W' \, (1 + 2\Delta q_M/q) \tag{B-23}$$

$$S'' = 4r \, \frac{|\Delta q_M|}{q} \left(\frac{1 + \Delta q_M/q}{1 + 2\Delta q_M/q} \right) \tag{B-24}$$

$$S' = r \, \frac{1}{(1 + 2\Delta q_M/q)} \quad . \tag{B-25}$$

Thus, all of the parameters necessary for computation of the intercepted areas are available, and for each point on the source disk the analysis problem is as follows: For any value of Δq_M we have three disks in the p-plane to consider--namely, W, W', and W'', which are shown in Fig. B-9. The size of these disks is completely independent

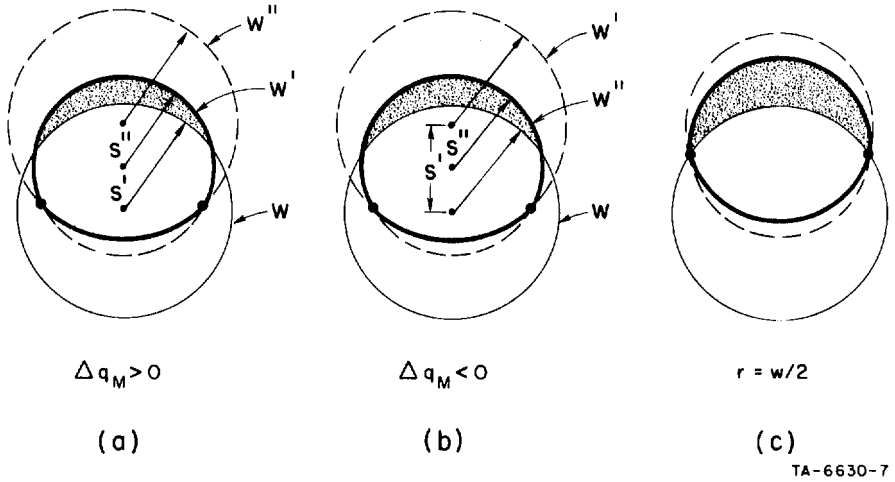

FIG. B-9 INTERCEPTED LIGHT PATTERS FOR POINT SOURCE WITHIN THE OBJECT DISK W

of r; however, their separations S' and S'' are a linear function of r. The light pattern falling on the p-plane has the shape of the common area between W' and W'', and the area of interest is the portion of this common area which falls outside the object disk W, shown shaded in Fig. B-9.

The computation of intercepted area A_I is greatly simplified because of an interesting geometric result (which is proven in Annex 2) that for $r < W/2$ the intersection of disks W' and W'' (identified in Fig. B-9 by large dots) always falls <u>within</u> the W circle, independent of the value of Δq_M. In the limit, for $r = W/2$, the W, W', and W'' circles intersect in the same two points, as depicted in Fig. B-9(c). Thus, the truncated portions of the returned light disk never in fact enter into the computation, and the intercepted area for $\Delta q_M > 0$ [Fig. B-9(a)] is given by

$$A_I = \pi W'^2/4 - A_c(W',W) \quad , \quad \text{for} \quad \Delta q_M > 0 \quad . \tag{B-26}$$

The intercepted area for $\Delta q_M < 0$ [Fig. B-9(b)] is given by

$$A_I = \pi W''^2/4 - A_c(W'',W) \quad , \quad \text{for} \quad \Delta q_M < 0 \quad . \tag{B-27}$$

To find the total intercepted light, we must multiply the intercepted area, as given in Eqs. (B-26) and (B-27), by the value of the illuminance of these areas. Note first that the illuminance (incident light flux per unit area) in the area A_I is the same as the illuminance E_p over the entire common area $A_c(W'',W')$, which is obtained by multiplying Eq. (B-10) (the illuminance of the corresponding area in the lens plane) by the inverse area ratio $[(p + \Delta p)/\Delta p]^2$, or

$$E_p = \frac{I_o dA}{\pi D'^2/4}\left(\frac{p + \Delta p}{\Delta p}\right)^2 = \frac{I_o dA}{D^2 \pi m^2 (\Delta q_M/q)^2} \quad . \tag{B-28}$$

Thus, the total intercepted light is

$$L_I = I_o \int_0^{W/2} \frac{A_I}{D^2 \pi m^2 (\Delta q_M/q)^2} 2\pi r dr \quad . \tag{B-29}$$

By substituting Eq. (B-26) into Eq. (B-29), normalizing A_I with respect to $\pi W'^2/4$, and writing D/W' in terms of $\Delta q_M/q$, we obtain the formula for intercepted light in the region $\Delta q_M > 0$:

$$L_I = I_o \int_0^{W/2} \frac{2\pi r}{\left(1 + \frac{2\Delta q_M}{q}\right)^2} \left[1 - \frac{A_c(W', W)}{\pi W'^2/4}\right] dr \quad , \quad \text{for } \Delta q_M > 0 \quad . \quad \text{(B-30)}$$

Similarly, substitution of Eq. (B-27) into Eq. (B-29) and normalization of A_I with respect to $\pi W''^2/4$ gives the intercepted light for $\Delta q_M < 0$:

$$L_I = I_o \int_0^{W/2} 2\pi r \left[1 - \frac{A_c(W'', W)}{\pi W''^2/4}\right] dr \quad , \quad 0.5\, q < q_M < 0 \quad . \quad \text{(B-31)}$$

When $\Delta q_M < q_{Mb}^-$, or $\Delta q_M > q_{Mb}^+$, none of the three circles intersect and $A_c(W', W) = A_c(W'', W) = \pi W^2/4$; therefore,

$$L_I = I_o A_W \left[\frac{1}{(1 + 2\Delta q_M/q)^2} - \left(\frac{\alpha}{2\Delta q_M/q}\right)^2\right] \quad ; \quad \Delta q_M > \Delta q_{Mb}^+ \quad \text{(B-32a)}$$

$$L_I = I_o A_W \left[1 - \left(\frac{\alpha}{2\Delta q_M/q}\right)^2\right] \quad ; \quad \Delta q_M < \Delta q_{Mb}^- \quad , \quad \text{(B-32b)}$$

where $A_W = \pi W^2/4$, the area of the object aperture. Thus it is clear that for large $\Delta q_M/q$, Eqs. (B-32) approach the values for total light return given in Eqs. (B-17) and (B-15), respectively. For interpreting the experimental curves shown below, it is of interest to note the values of L_I at the Δq_{Mb} points; these are obtained by substitution of the values of Δq_{Mb}^+ and Δq_{Mb}^-, respectively, into Eqs. (B-32a) and (B-32b):

$$L_I = I_o A_W \left[\frac{1 - \alpha^2}{1 + \alpha^2} - \frac{1 - \alpha^2}{4}\right] \quad , \quad \text{for } \Delta q_M = \Delta q_{Mb}^+ \quad \text{(B-33a)}$$

$$L_I = I_o A_W \left[1 - \frac{1 - \alpha^2}{4}\right] \quad , \quad \text{for } \Delta q_M = \Delta q_{Mb}^- \quad . \quad \text{(B-33b)}$$

For small values of α, the intercepted light at both Δq_{Mb} points is very close to 75 percent of the maximum light return.

It should be noted from Eqs. (B-22) through (B-25), that if all dimensions are normalized in terms of W, then the significant parameter of the system is α, as given by Eq. (B-14). To verify experimental measurements of L_T and L_I as functions of Δq_M, the integrals of

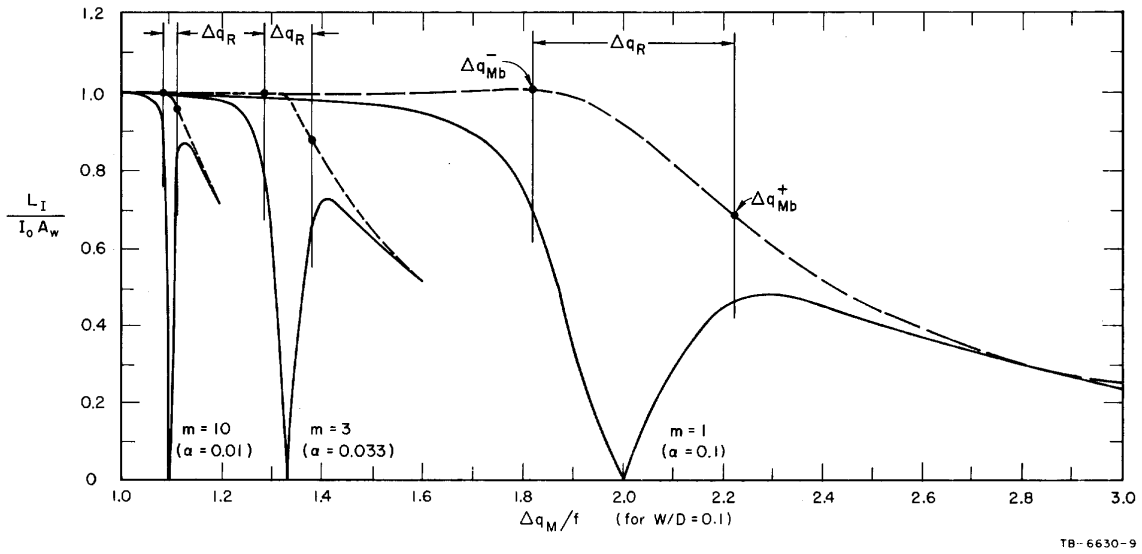

FIG. B-10 COMPUTED VALUES OF INTERCEPTED LIGHT AS A FUNCTION OF MIRROR POSITION
(a) Δq normalized with respect to focal length at a given W/D ratio

Eqs. (B-12), (B-30), and (B-33) were computed for three values of α, and the results are plotted in Fig. B-10. The values of Δq_{Mb}^{+} and Δq_{Mb}^{-} are indicated on each of the curves of Fig. B-10(a). From these curves it is clear that these points do in fact encompass the "sensitive region" for intercepted light around the in-focus point. Thus, we can specify the range of focus detection as

$$\Delta q_R = \Delta q_{Mb}^{+} - \Delta q_{Mb}^{-} \tag{B-34}$$

$$\Delta q_R = \left(\frac{2\alpha}{1 - \alpha^2}\right) q \quad . \tag{B-35}$$

The variations of L_I with Δq_M normalized with respect to Δq_R are plotted in Fig. 10(b).

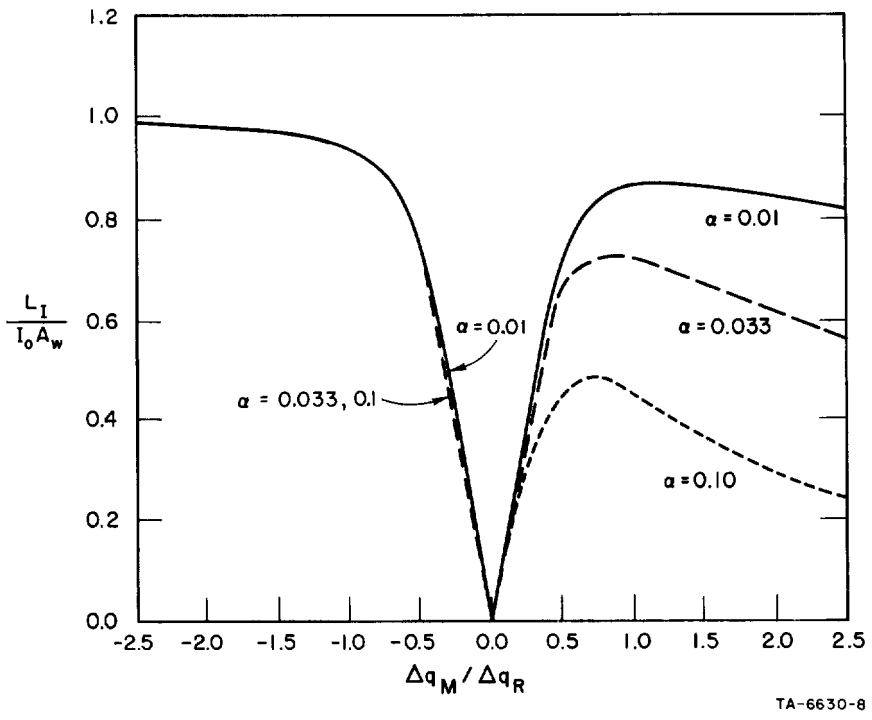

FIG. B-10 COMPUTED VALUES OF INTERCEPTED LIGHT AS A FUNCTION OF MIRROR POSITION
(b) Δq normalized with respect to Δq_R

By substituting in Eq. (B-35) the expression $[(m + 1)/m]f$ for q, which is readily derived from the basic lens equation, we obtain an expression for range in terms of more commonly used optical parameters, namely,

$$\Delta q_R = \frac{2(m + 1)}{m^2 - W^2/D^2} W \cdot F \qquad \text{(B-36)}$$

where F is the f-number of the lens (i.e., F = f/D). If $\alpha \ll 1$ then

$$\Delta q_R \approx 2 \frac{W \cdot F}{m} \quad . \qquad \text{(B-37)}$$

Experimentally measured curves of intercepted light are shown in Fig. B-11 for values of α very close to those computed above. The sharpness of the nulls is reduced in the experimental curves because of

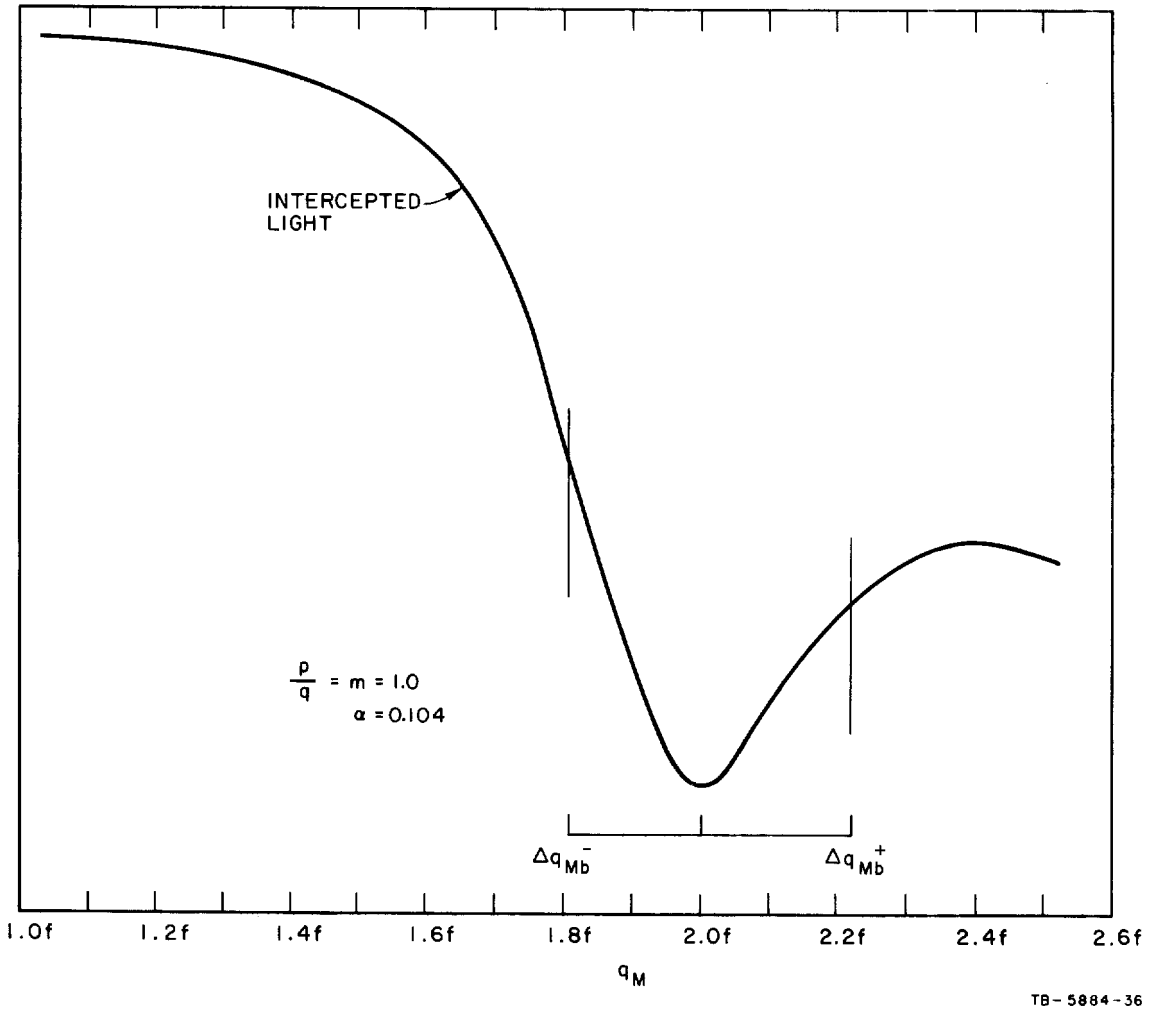

FIG. B-11 EXPERIMENTALLY MEASURED INTERCEPTED LIGHT FOR THREE VALUES OF α

various optical-system distortions and stray light pickup, though it is clear that there is extremely good correlation between the experimental and theoretical curves, especially with regard to the width of the central dip zone and the position of the maximum for $\Delta q_M > 0$.

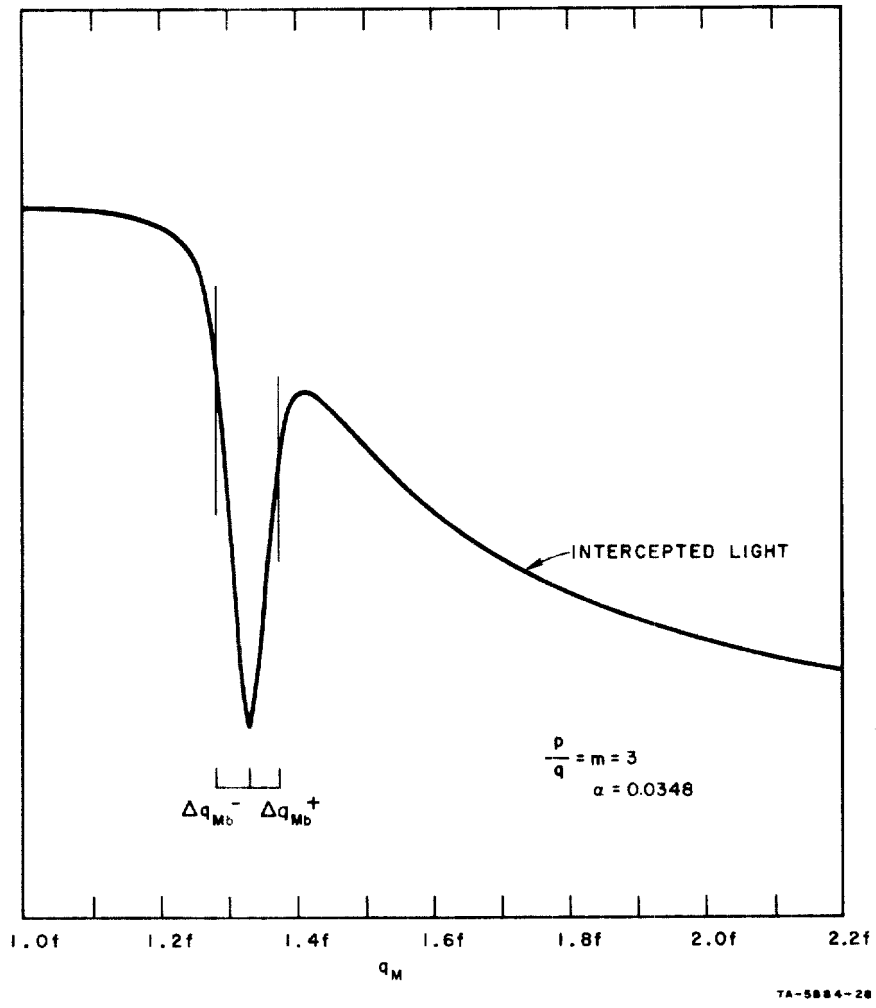

FIG. B-11 Continued

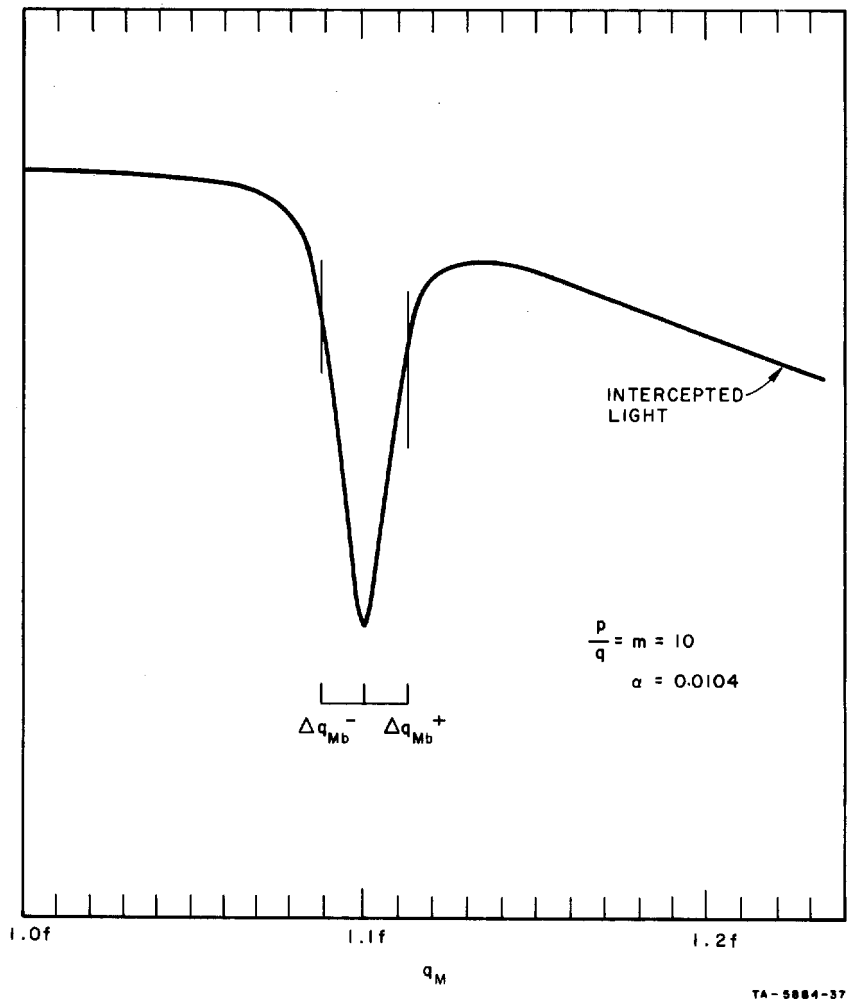

FIG. B-11 Concluded

4. EFFECTS OF MISALIGNMENT

The reciprocal imaging technique ensures that (except for second-order effects) the return image will be perfectly aligned with the source object when $\Delta q_M = 0$, independent of the lateral position of the source and angular position of the reflecting surface. Thus, if this technique is used to detect the position of some reflective surface (e.g., a photographic film), we should be able to tolerate some amount of misalignment of film or source with respect to the lens, without causing significant focus detection error. Of course, extreme errors in alignment will cause serious reduction in the total returned light L_T, and change the form of the intercepted light L_I as a function of Δq_M. For both types of misalignment, extreme points exist beyond which no light at all is returned through the lens. In the case of an off-axis displacement d of a circular disk source of diameter W, the extreme point, for the case $\Delta q_M = 0$, occurs at

$$d' = m \frac{W}{2} (1 + \alpha) \quad , \tag{B-38}$$

i.e., for $d > d'$ the total returned light is zero. Figure B-12 shows the experimentally determined modification produced in the L_I curve by a misalignment corresponding to 1/2 d', for m = 3.

In the case of angular misalignment the extreme point for $\Delta q_M = 0$ is given by θ_c, where

$$\theta_c = \tan^{-1} \left(\frac{1}{2F} \left[\frac{1 + \alpha}{1 + m} \right] \right) \tag{B-39}$$

where F is the f-number (f/D) of the lens. The measured curves of Fig. B-13 show the effect on L_I for various values of angular misalignment of the reflecting surface. For these curves the source disk is centered and the reflecting surface is rotated about an axis that passes orthogonally through the optic axis.

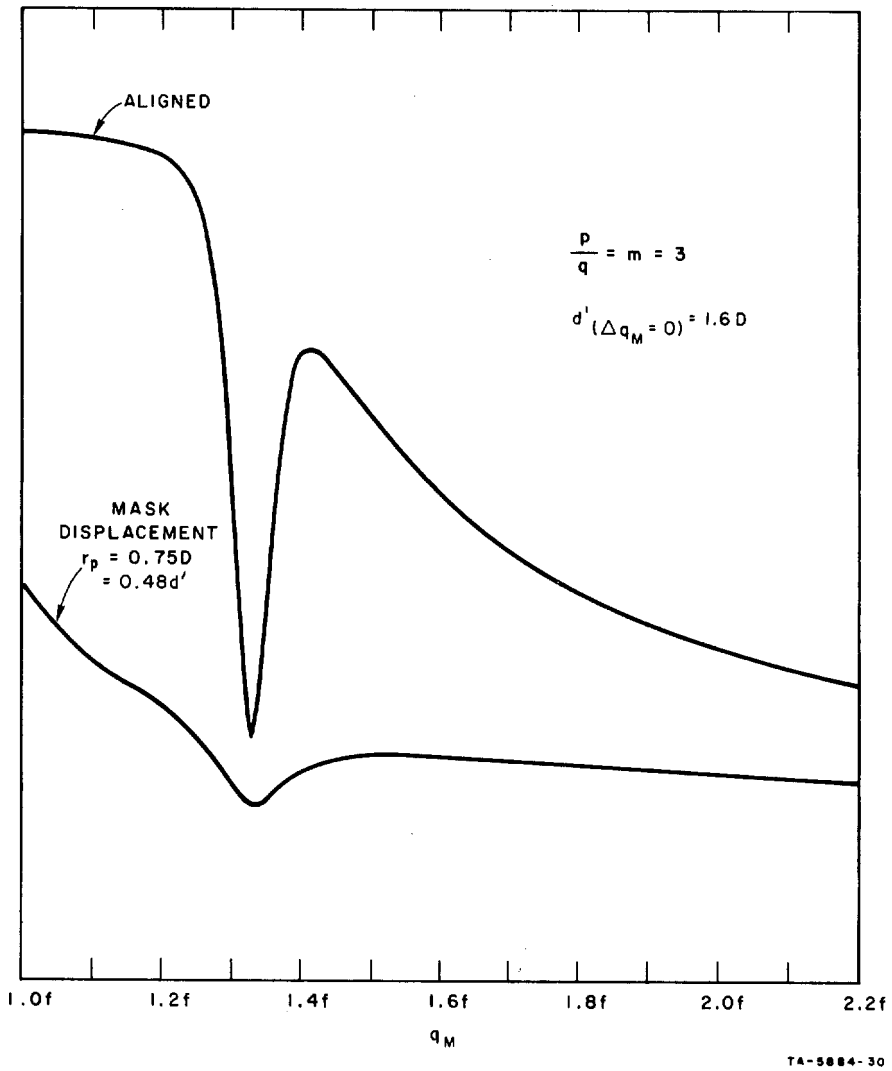

FIG. B-12 RESPONSE WITH MASK OFF AXIS

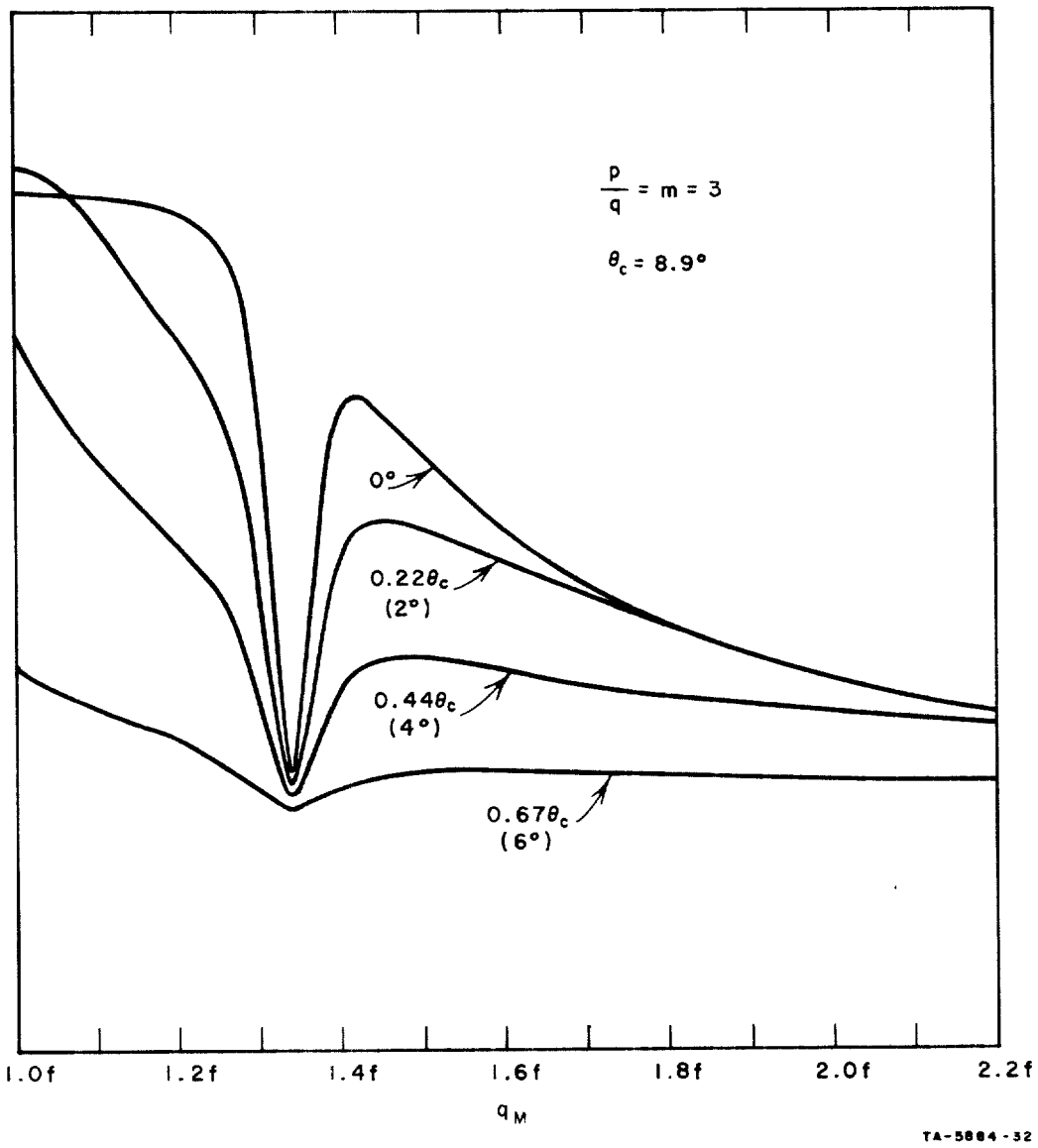

FIG. B-13 EFFECT OF ANGULAR DISPLACEMENT OF FILM SURFACE

5. DISCUSSION

We have described a reciprocal, self imaging, optical system for monitoring the position of a reflecting mirror surface. The technique involves the projecting of a pattern onto the mirror surface, by means of a lens, and having the reflection reimaged onto the original pattern. If the first image is exactly in focus on the reflecting surface, then by optical reciprocity, the returned image ideally falls exactly on the original source pattern. As the reflecting surface moves out of the image plane, the returned image is correspondingly defocused and part of the returned light falls beyond the input pattern and is intercepted by the monitoring system. Thus, the intercepted light is nominally zero with the mirror in the image plane, and increases with mirror movement away from the image plane in either direction. It is the position that corresponds to minimum intercepted light, therefore, that represents optimum focus in the monitoring system, and mirror movements away from this position are readily detected.

We analyze the case of a uniformly illuminated circular disk input pattern, formed by illumination of a circular cutout in an opaque sheet. For purposes of experimental evaluation, the intercepted light is measured by a photocell that detects the light falling onto the surface of the opaque sheet facing the lens.

Only for a circular input pattern and circular lens aperture is the system easily analyzed, and the theoretical and experimental curves for this case are in very good agreement. Of primary interest for design of such a system is the width of the sensitive "dip region" of intercepted light, and one of the more interesting nonintuitive results of the analysis is that this region is determined by a single parameter $\alpha = (W/mD)$, where (W/D) is the ratio of input-image diameter to lens diameter, and m is the magnification (p/q) in the optical system. In terms of α, the width of the dip region is shown to be on the order of $2\alpha q$, where q is the lens to mirror distance. Computed and experimental plots for several different values of α are shown. It is also shown that the minimum-dip position is insensitive to reasonably large

rotations of the mirror surface, and reasonably large lateral movements of the input pattern.

For small values of α, the detection range is correspondingly small, but the system becomes very sensitive to small displacements of the reflecting surface. If, in Eq. (B-37), the lens f-number F = 1 and m = 10, then the total detection range Δq_R for an input disk W = 1 mm is 0.1 mm = 100 microns. As noted in Eq. (B-33), the light intercepted at the ends of the range (at Δq_{Mb}^- and Δq_{Mb}^+) is nearly 75 percent of the maximum return, so that with this system we should be able to sense displacements of at least 1/10 of this range, or 10 microns, and possibly as little as 1 micron.

Annex 1

COMMON AREA OF CIRCLES OF DIFFERENT DIAMETERS

The common area $A_c(r,R)$ between two circles having different radii r and R, and relative separation S (see Fig. B-14), is derived by means of the double integration

$$A_c(r,R) = 2 \int_0^{R\cos\theta} dx \int_{S-\sqrt{r^2-x^2}}^{\sqrt{R^2-x^2}} dy \qquad \text{(B-40)}$$

where θ is the angle shown in Fig. B-14. The relation between θ and S is derived from

$$S = r \sin \alpha + R \sin \theta \qquad \text{(B-41)}$$

and

$$R \cos \theta = r \cos \alpha \quad . \qquad \text{(B-42)}$$

Substituting Eq. (B-42) into Eq. (B-41), we find

$$S = r\sqrt{1 - \left(\frac{R}{r}\right)^2 \cos^2 \theta} + R\sqrt{1 - \cos^2 \theta} \qquad \text{(B-43)}$$

from which we find

$$\cos^2 \theta = 1 - \left[\frac{S^2 + R^2 - r^2}{2SR}\right]^2 \quad . \qquad \text{(B-44)}$$

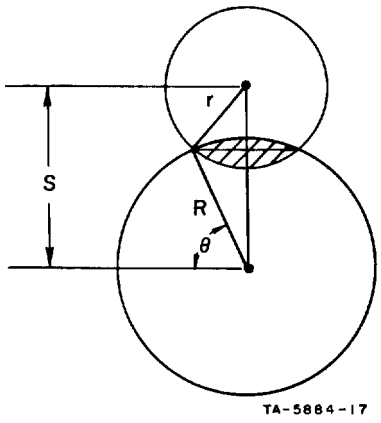

FIG. B-14 ARRANGEMENT FOR COMPUTING COMMON AREA BETWEEN TWO UNEQUAL OVERLAPPING DISKS

The indefinite integral of the function $\sqrt{a^2 - x^2}$ is

$$\int \sqrt{a^2 - x^2}\, dx = \frac{1}{2}\left[x\sqrt{a^2 - x^2} + a^2 \sin^{-1}\left(\frac{x}{a}\right)\right] \quad . \qquad \text{(B-45)}$$

Applying Eq. (B-44) to Eq. (B-40), we obtain

$$A_c(r,R) = R^2\cos\theta\left[-\sqrt{1 - \cos^2\theta} + \sqrt{\left(\frac{r}{R}\right)^2 - \cos^2\theta} - \frac{2S}{R}\right] + R^2\sin^{-1}(\cos\theta) + r^2\sin^{-1}\left(\frac{R\cos\theta}{r}\right) \quad , \tag{B-46}$$

which can be converted by means of Eq. (B-44) to the form

$$A_c(r,R) = - RS\cos\theta + R^2\sin^{-1}(\cos\theta) + r^2\sin^{-1}\left(\frac{R\cos\theta}{r}\right) \quad . \tag{B-47}$$

Note that for r = R and S = 0, Eq. (B-44) correctly predicts that cos θ = 1 (or θ = 0), and Eq. (B-47) correctly predicts $A = \pi R^2$. Also, for r = R, and S = 2R (i.e., externally tangent circles), Eq. (B-44) correctly predicts cos θ = 0 (or θ = π/2) and Eq. (B-47) correctly predicts A = 0.

Now we must note that Eq. (B-45) applies only for $S \geq S_c$ where $S_c = \sqrt{R^2 - r^2}$. How this limitation comes about can be seen from Fig. B-15(a). When $S = S_c$, the center of the smaller circle lies exactly on the common chord of intersection. This case represents the largest possible chord of intersection, namely, the diameter of the smaller circle. For $S < S_c$, the integral in Eq. (B-40) is incomplete, since it accounts only for the area bounded by the heavy lines in Fig. B-15(b), but not the cross-hatched areas. The area A′ of the cross-hatched

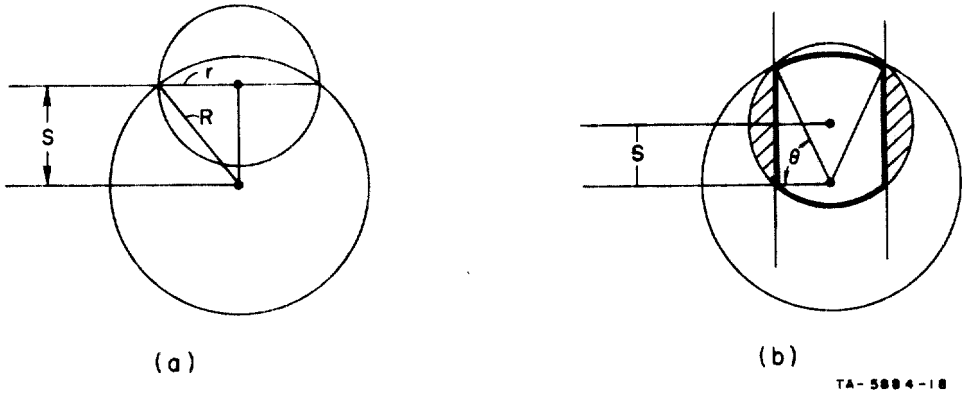

FIG. B-15 COMPUTATION OF OVERLAP AREA FOR SMALL VALUES OF SEPARATION

regions is readily evaluated from

$$A' = 4 \int_{R\cos\theta}^{r} \sqrt{r^2 - x^2}\, dx \quad , \tag{B-48}$$

which, by application of Eq. (B-45), reduces to

$$A' = \pi r^2 - 2R^2 \cos\theta \left[\sqrt{\left(\frac{r}{R}\right)^2 - \cos^2\theta}\right] - 2r^2 \sin^{-1}\left(\frac{R\cos\theta}{r}\right) \quad . \tag{B-49}$$

Adding A' to Eq. (B-47) and simplifying, we obtain for $0 \leq S \sqrt{R^2 - r^2}$

$$A_c(r,R) = -RS\cos\theta + R^2 \sin^{-1}(\cos\theta) + r^2 \left[\pi - \sin^{-1}\left(\frac{R\cos\theta}{r}\right)\right] \quad . \tag{B-50}$$

Note that for $S = \sqrt{R^2 - r^2}$, Eq. (B-44) correctly predicts $\cos\theta = r/R$, and Eqs. (B-46) and (B-50) predict the identical value of common area, namely,

$$A_c = \frac{\pi r^2}{2} - r\sqrt{R^2 - r^2} + R^2 \sin^{-1}\left(\frac{r}{R}\right) \quad , \tag{B-51}$$

which in turn predicts the correct value of A_c as $R \to \infty$, since the common arc through the smaller circle then approaches a straight line segment, and we expect simply that $A_c \to \pi r^2/2$.

Figure B-16 shows a set of computer results for various ratios of R/r. Note that for R/r = 20 the curve is almost symmetric, as it should be for $R/r \to \infty$. For R = r, the curve is remarkably linear. The curve shape changes rapidly with small increases in R/r, the R/r = 2 curve lying almost halfway between the R/r = 1 and R/r = 20 curves.

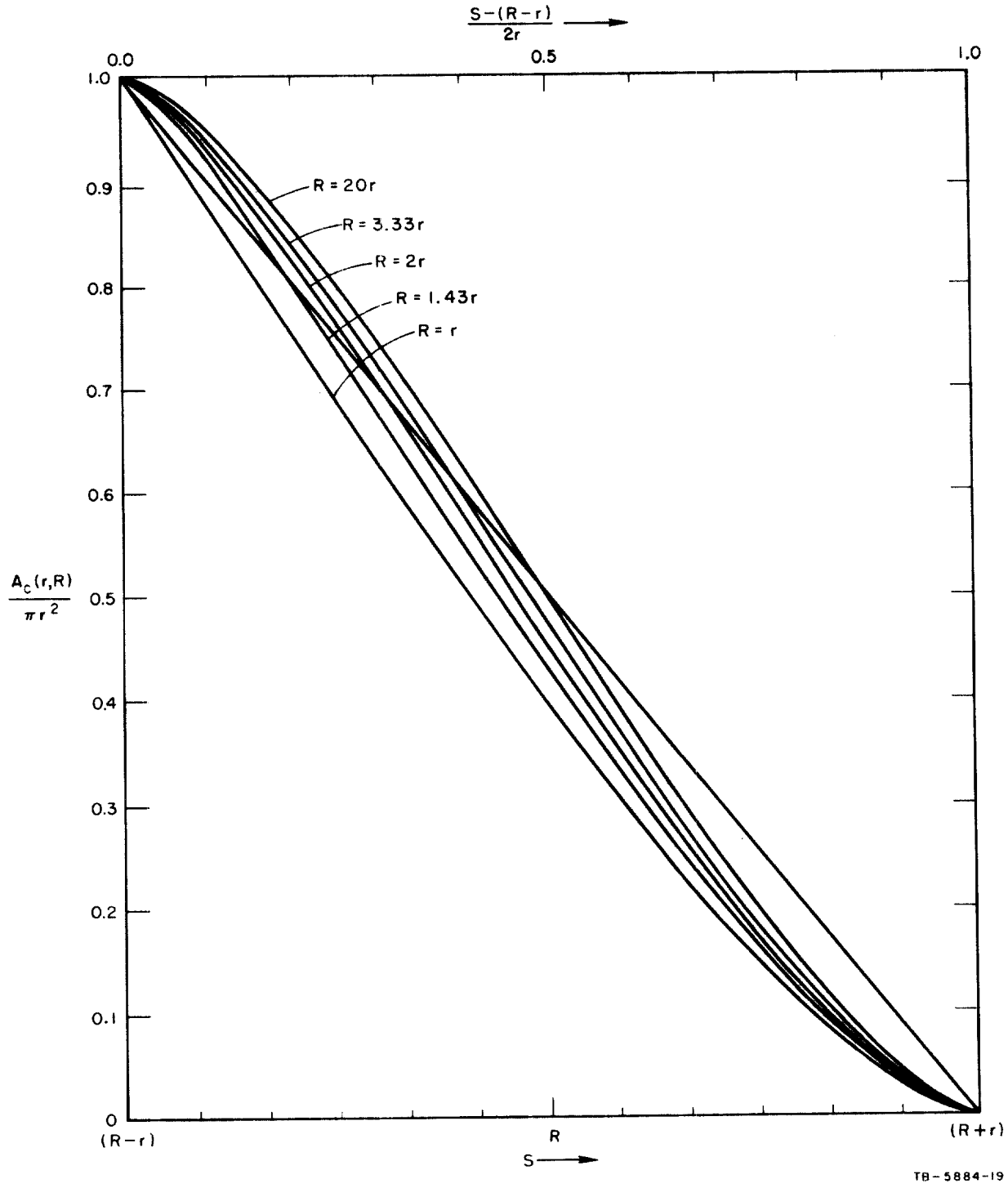

FIG. B-16 COMPUTER-GENERATED CURVES OF COMMON AREA AS A FUNCTION OF SEPARATION S OVER THE RANGE $R - r < S < R + r$ FOR DIFFERENT RADIUS RATIOS

Annex 2

PROOF THAT THE W′ AND W′′ DISKS INTERSECT WITHIN THE W DISK FOR ALL Δq_M

In order to locate the points of intersection of the W′ and W′′ circles with respect to the object disk W, a triangle is formed by joining the centers of the W and W′ circles with the point of intersection of W and W′, as shown in Fig. B-17(a) for the case $\Delta q_M < 0$. We can write the following expression for the angle Φ, in terms of the three known sides (S′ - S′′), W′′/2, W/2,

$$(W''/2)^2 = (S' - S'')^2 + (W/2)^2 - 2(S' - S'')(W/2)\cos\Phi \quad , \quad (\Delta q_M < 0) \tag{B-52}$$

which, upon substitution of Eqs. (B-23), (B-24), and (B-25) for W′′, S′′, and S′, takes the form

$$\left(\frac{\Delta q_M}{q}\frac{W}{\alpha}\right)^2 = r^2\left(\frac{2\Delta q_M}{q} + 1\right)^2 + \left(\frac{W}{2}\right)^2 - rW\left(\frac{2\Delta q_M}{q} + 1\right)\cos\Phi \quad , \tag{B-53}$$

or

$$\cos\Phi = \frac{(W/2)^2 + r^2\left(\frac{2\Delta q_M}{q} + 1\right)^2 - \left(\frac{W}{\alpha}\frac{\Delta q_M}{q}\right)^2}{rW\left(\frac{2\Delta q_M}{q} + 1\right)} \quad , \quad \text{for} \quad (\Delta q_M < 0) \quad . \tag{B-54}$$

We next consider the triangle extended to include the center of the W′′ circle; this triangle shares the same angle Φ, but in the extended triangle the adjacent sides are of length S′ and W′/2. We can now compute the length of side T, which is opposite angle Φ, and note that if W′/2 is greater than T, then the points of intersection of W′ and W′′ must fall inside W, and if T = W′/2, the circles share one common chord of intersection [as in Fig. B-9(c)]. The value of T can be found from

$$T^2 = (S')^2 + (W/2)^2 - 2S'(W/2)\cos\Phi \quad , \tag{B-55}$$

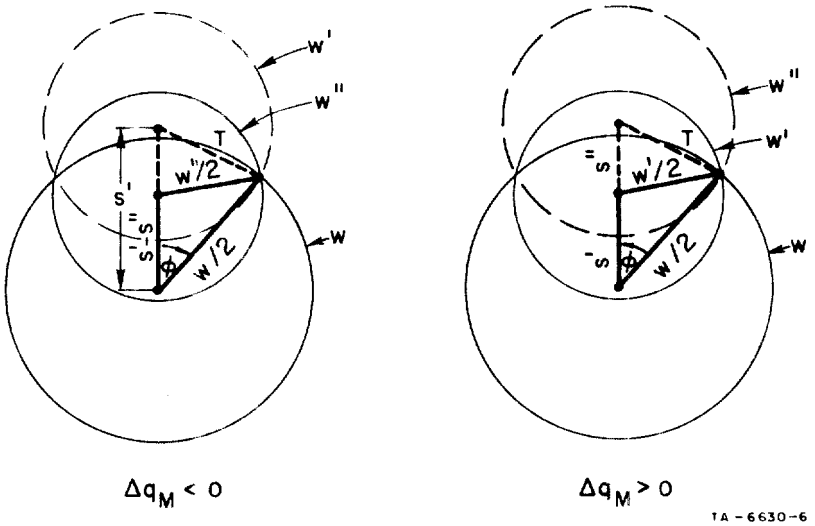

FIG. B-17 RELATIONSHIP BETWEEN W, W', W" CIRCLES IN THE OBJECT PLANE

or

$$T^2 = \frac{r^2}{\left(1 + \frac{2\Delta q_M}{q}\right)^2} + \frac{W^2}{4} - \frac{rW}{\left(1 + \frac{2\Delta q_M}{q}\right)} \cos \Phi \quad , \qquad \text{(B-56)}$$

which upon substitution of Eq. (B-54) becomes

$$T^2 = \frac{(W^2 - 4r^2)\left(1 + \frac{2\Delta q_M}{q}\right)^2 - (W^2 - 4r^2) + 4\left(\frac{\Delta q_M}{q}\frac{W}{\alpha}\right)^2}{4\left(1 + \frac{2\Delta q_M}{q}\right)^2} \quad . \qquad \text{(B-57)}$$

From Eq. (B-22) we obtain the value of $W'/2 = (W/\alpha\ \Delta q_M/q)/(1 + 2\Delta q_M/q)$; this quantity is squared and subtracted from Eq. (B-57) to obtain

$$T^2 - W'^2/4 = (W^2 - 4r^2)\frac{\Delta q_M}{q}\left(\frac{1 + \Delta q_M/q}{1 + 2\Delta q_M/q}\right) \quad , \quad \Delta q_M < 0 \quad . \qquad \text{(B-58)}$$

For $r = W/2$, $(T^2 - W'^2/4) = 0$ for all values of Δq_M in the range $-0.5 < \Delta q_M/q < 0$, and we have the interesting result that all three circles intersect in the same two points. For $r < W/2$, the magnitude of $(T^2 - W'^2/4)$ is negative for all Δq_M in the same range, and, thus, the points of intersection of W' and W'' always lie within, or just on, the W disk.

We now show that the same conclusion holds for $\Delta q_M > 0$; in this case Fig. B-17(b) applies, and the following equations may be written:

$$(W'/2)^2 = S'^2 + (W/2)^2 - 2S''(W/2)\cos\Phi \quad , \tag{B-59}$$

$$\cos\Phi = \frac{r^2 + (W/2)^2\left(1 + \frac{2\Delta q_M}{q}\right)^2 - \left(\frac{W}{\alpha}\frac{\Delta q_M}{q}\right)^2}{rW\left(1 + \frac{2\Delta q_M}{q}\right)} \quad . \tag{B-60}$$

The side T of the extended triangle is now given by

$$T^2 = (S' + S'')^2 + (W/2)^2 - 2(S' + S'')(W/2)\cos\Phi \quad , \tag{B-61}$$

or

$$T^2 = -(W^2 - 4r^2)\frac{\Delta q_M}{q}\left(1 + \frac{\Delta q_M}{q}\right) + \left(\frac{W}{\alpha}\frac{\Delta q_M}{q}\right)^2 \quad . \tag{B-62}$$

Subtracting $W''^2/4$ from T^2, we obtain

$$(T^2 - W''^2/4) = -(W^2 - 4r^2)\frac{\Delta q_M}{q}\left(1 + \frac{\Delta q_M}{q}\right) \quad , \quad \text{for} \quad (\Delta q_M > 0) \quad . \tag{B-63}$$

For all values of $\Delta q_M > 0$, the value of $(T^2 - W''^2/4)$ is negative for $r < W/2$, so that again the intersection of W' and W'' is within the W disk, and again for $r = W/2$, we have $T = W''/2$ and the circles intersect exactly on the W circle.

Appendix C

DETERMINATION OF RECEPTOR SIZE NEEDED TO RECEIVE INTERCEPTED LIGHT

For $\Delta q_M > 0$

Light will extend as far out as the edge of the W'' disk (see Fig. B-9); the edge of the W'' disk is furthest extended for input points at $r = W/2$. The distance of the edge of the W'' disk from the optic axis is

$$\ell = S' + S'' + W''/2 = \text{radius of required collection area.} \qquad \text{(C-1)}$$

Using Eqs. (B-25), (B-24), and (B-23), we obtain

$$\ell = \frac{r}{1 + 2\,\frac{\Delta q_M}{q}} + \frac{4r\,\frac{\Delta q_M}{q}\left(1 + \frac{\Delta q_M}{q}\right)}{1 + 2\,\frac{\Delta q_M}{q}} + W'(1 + 2\,\Delta q_M/q) \quad , \qquad \text{(C-2)}$$

or, at $r = W/2$

$$\ell = \frac{W}{2}\,\frac{1 + 4\,\frac{\Delta q_M}{q} + 4\left(\frac{\Delta q_M}{q}\right)^2}{1 + 2\,\frac{\Delta q_M}{q}} + \frac{W}{\alpha}\,2\,\frac{\Delta q_M}{q} \qquad \text{(C-3)}$$

$$\ell = \frac{W}{2}\left[\left(1 + 2\,\frac{\Delta q_M}{q}\right) + \frac{4}{\alpha}\,\frac{\Delta q_M}{q}\right] \qquad \text{(C-4)}$$

$$\ell = \frac{W}{2}\left[1 + 2\,\frac{\Delta q_M}{q}\left(1 + \frac{2}{\alpha}\right)\right] \qquad \text{(C-5)}$$

For $\Delta q_M = \Delta q_{Mb^+} = \frac{\alpha}{1 - \alpha}$, then

$$\ell = \frac{W}{2}\left[1 + \frac{2\alpha}{1 - \alpha} + \frac{4}{1 - \alpha}\right] \qquad \text{(C-6)}$$

$$= \frac{W}{2}\left(\frac{5 + \alpha}{1 - \alpha}\right) \qquad \text{(C-7)}$$

For $\Delta q_M < 0$

In this case, light will extend to the edge of the W' disk, and ℓ is then

$$\ell = S' + |W'/2| \tag{C-8}$$

Then using Eqs. (B-25) and (B-22)

$$\ell = \frac{r}{1 + 2\,\dfrac{\Delta q_M}{q}} + \left| \frac{W}{2\alpha} \, \frac{2\,\dfrac{\Delta q_M}{q}}{1 + \dfrac{\Delta q_M}{q}} \right| \tag{C-9}$$

For $r = W/2$

$$\ell = \frac{W}{2} \left[\frac{1 + \left| \dfrac{2}{\alpha} \, \dfrac{\Delta q_M}{q} \right|}{1 + 2\,\dfrac{\Delta q_M}{q}} \right] \tag{C-10}$$

Again, for $\Delta q_M = \Delta q_{Mb}^{-} = \dfrac{-\alpha}{1 + \alpha}$

$$\ell = \frac{W}{2} \left[\frac{1 + \dfrac{2}{1 + \alpha}}{1 - \dfrac{2\alpha}{1 + \alpha}} \right]$$

$$= \frac{W}{2} \left(\frac{3 + \alpha}{1 - \alpha} \right) \tag{C-11}$$

Appendix D

CALCULATION OF DETECTION GAIN

From Fig. B-10 in Appendix B, it is clear that if $I_o A_W$ is constant, the sensitivity of the intercepted light to motions in the film plane (in the range $-0.5\ \Delta q_R$ to $0.5\ \Delta q_R$) does not change significantly with α. Effects of changes in magnification and geometry on $I_o A_W$ will determine how the gain (light change per unit motion of film) of the intercepted light function changes. I_o is the illuminance at the center of the returned image with the film in the in-focus position; this is given by

$$I_o = \pi B_s \frac{1}{1 + 4(m + 1)^2 F^2} \qquad \text{(D-1)}$$

where B_s is the uniform diffuse luminance of the source (lumens/m^2/steradian). Therefore, the quantity $I_o A_W$ is

$$I_o A_W = \pi^2 B_s \frac{W^2}{1 + 4(m + 1)^2 F^2} \approx \frac{W^2}{4m^2 F^2} \quad (m \gg 1) \quad . \qquad \text{(D-2)}$$

Thus, if m is increased, and F and Δq_R are kept constant, the latter requires that W must increase linearly with m. Equation (D-2) states that, under these conditions, $I_o A_W$ (and, therefore, the detection gain) remains constant.

Next 1 Page(s) In Document Exempt

Approved For Release 2003/01/28 : CIA-RDP78B04770A002000040013-3